Age and structure of the San Jacinto and San Felipe fault zones, and their lifetime slip rates

Susanne Janecke[1], Becky Dorsey[2], and Benjamin Belgarde[1,3]
[1]*Department of Geology, Utah State University, Logan, UT 84322-4505*
(susanne.janecke@usu.edu)
[2]*University of Oregon*
[3]*ExxonMobil, Houston TX*

Contributors:
D. Forand, B. Housen, S. Kirby, V. Langenheim, A. Lutz, T. Rittenour, and A. Steely

PART 1: BACKGROUND AND STATEMENT OF PROBLEM

Background and Statement of Problem

The San Jacinto and San Felipe dextral strike-slip fault zones are important for understanding plate-boundary dynamics, regional slip partitioning, and seismic hazards in southern California (Figs. 1, 2). However, their age of initiation and long-term average slip-rates are controversial, and little is known about the structural evolution of these fault zones during their short geologic history. Research by our group over the past ~6 years has addressed these questions with the goal of understanding the age and geological evolution of these fault zones, and their influence on Plio-Pleistocene regional stratigraphy and basin development in the western Salton Trough. A second major question concerns the distribution of strain within the evolving fault zones, particularly in the basinal deposits where prior studies found limited evidence for a significant displacement on the southeastward extension of the Clark fault (Figs. 3, 4, 5 and 6).

The age of the San Jacinto fault zone has been debated over the past ~15 years. One popular model concluded that the San Jacinto zone formed ca. 2-2.5 Ma, based on late Quaternary slip rates of ~9-12 mm/yr at Anza (Sharp, 1967; Rockwell et al., 1990). This rate requires about 2 to 2.5 m.y. to produce the 24-29 km of right slip on the fault (e.g. Sharp, 1967; Hill, 1984). Indirect support for this age was derived from an anticline in the western San Bernardino Mountains that was originally thought to have initiated ~ 2-2.5 Ma near the subsurface branch point between the San Andreas and San Jacinto fault (Table 1) (Meisling and Weldon, 1989; Weldon et al., 1993; Morton and Matti, 1993; Rockwell et al., 1990; Rockwell, pers. comm., 2003; Weldon pers. comm., 2002).

In contrast, stratigraphic and structural studies in the San Timoteo Badlands near San Bernardino concluded that contraction and structural complexities in San Gorgonio Pass resulted in initiation of the San Jacinto fault zone between 1.4 and 1.2 Ma, to partially bypass

In Clifton, H.E., and Ingersoll, R.V., eds., 2010, Geologic excursions in California and Nevada: tectonics, stratigraphy and hydrogeology: Pacific Section, SEPM (Society for Sedimentary Geology) Book 108, p. 233-271.

the eastern 55 km of the Big Bend in the San Andreas fault (Matti and Morton, 1993; Morton and Matti, 1993; Albright, 1999). The faster implied slip rate was subsequently supported by a study in the San Timoteo Badlands by Kendrick et al. (2002), in which a Pleistocene slip rate of ca. 20 mm/yr over the past ~100 k.y. was deduced from rates of active uplift and erosion adjacent to the San Jacinto fault (Table 1). In addition, a recent integrated GPS and InSar inversion study by Fialko (2006) yielded a modern slip rate of 19-21 mm/yr across the San Jacinto fault zone in the Salton Trough. These results could reflect changing slip rates over time but also raise the possibility that there may be no significant or resolvable differences between geologic, Holocene, and modern slip rates in the San Jacinto fault zone.

The large disparity between slip rates derived from different data sets for different timescales has motivated our study to determine the age of initiation and long-term slip rates for the San Jacinto and San Felipe fault zones in the western Salton Trough (Tables 1 and 2). We emphasize that the age of these fault zones must be deduced from stratigraphic, structural, and other geologic data in and adjacent to the fault zones. Their ages cannot be assumed from extrapolation of young slip rates over geologic timescales, because it is well known that slip rates can and commonly do vary over time. This is a geological problem that must be solved with field-based geologic studies.

Our research has also considered whether there is significant off-fault displacement in the damage zone of strike-slip faults that might explain the discrepancies between higher GPS-based slip rates and slower slip rates based on paleoseismic studies and offset geomorphic features (Belgarde, 2007; D. Forand, in revision)(Table 1 and Le et al., in press). One objective of this field trip is to illustrate the extremely distributed strain of the southeastern two structural segments of the Clark fault, and to show that there is significant hidden strain on these structures that is both Quaternary in age and coseismic.

Summary of Results

Since 2002, S. Janecke, R. Dorsey, and their students and colleagues have carried out a series of detailed mapping, stratigraphic, structural, and paleomagnetic studies of Plio-Pleistocene sedimentary and older crystalline rocks in the San Jacinto and San Felipe fault zones. These studies produced four completed masters theses (Belgarde, 2007; Kirby, 2005; Lutz, 2005; Steely, 2006), one in progress (Forand, in revision), three papers (Lutz et al., 2006; Kirby et al., 2007; Steely et al., 2009), and one large synthesis paper in revision (Janecke et al., in revision GSA Special Paper). The main results and highlights of these studies are briefly summarized below with an emphasis on the newer and unpublished results in Janecke et al. (in revision) and two prepublication manuscripts by Janecke and Belgarde in Belgarde (2007). Please refer to the papers themselves for additional detail and figures.

Stratigraphic Studies

The Pleistocene Ocotillo Formation and its eastern distal equivalent, the Brawley Formation, make up a widespread unit of conglomerate and sandstone that rests on older lacustrine deposits of the Borrego Formation in the western Salton Trough (Figs. 3, 5, and 6). Magnetostratigraphic analysis shows that the base of the Ocotillo Formation in the western Borrego Badlands is 1.05 ± 0.03 Ma (Lutz et al., 2006), and the base of the Brawley Formation in the eastern San Felipe Hills is the same age and in both places the contact is coincident with the base of the Jaramillo subchron (Kirby et al., 2007). The correlative base of the Ocotillo and

Brawley formations varies from a slight hiatus marked by soil development in the Borrego Badlands, to a sharp disconformity in the San Felipe Hills, to a prominent angular unconformity roughly coinciding with the San Felipe anticline in the western San Felipe Hills. The Ocotillo Formation reveals an up-section increase in calcite-cemented, quartz-rich sandstone clasts derived from the Pliocene Arroyo Diablo Formation, a widespread unit derived from the Colorado River that accumulated during slip on the West Salton detachment fault.

The above data show clearly that the laterally equivalent Ocotillo and Brawley formations record rapid, nearly simultaneous progradation of coarse alluvial and fluvial clastic sediments ~25-30 km to the east and NE across a former large perennial lake represented by mud-rich lacustrine deposits of the Borrego Formation. We have considered and rejected a climatic explanation for progradation of the Borrego-Brawley unit because: (1) the age is too young to be the result of global climate change that resulted from onset of northern hemisphere glaciation at ~2.5-3 Ma; (2) climate change cannot explain the angular unconformity that is locally developed at the base of the Ocotillo Formation; and (3) climate forcing also cannot explain the presence of sandstone clasts reworked from the older Arroyo Diablo Formation, which requires structural inversion uplift and erosion of a basin that previously formed in the hanging wall of the West Salton detachment fault. The Ocotillo and Brawley formations accumulated in a large subsiding depocenter influenced by basin-bounding faults and intrabasinal structures between ~1.1 and 0.5-0.6 Ma (Lutz et al., 2006). Subsidence ended at 0.5-0.6 Ma, resulting in deposition of the thin Fonts Point Sandstone starting at ~0.6 Ma (Lutz et al., 2006). The Fonts Point Sandstone was possibly the oldest pediment deposit to form in this region after widespread subsidence and deposition ceased. It was subsequently uplifted and now serves as a useful strain marker for active faulting and folding that has been ongoing for the past ~ 500 ka.

Based on the points summarized above, we conclude that rapid progradation of the Ocotillo and Brawley formations was driven by a dramatic increase in sediment flux from the eastern Peninsular Ranges, including inverted parts of the former supradetachment basin of the West Salton detachment fault. Relationships in the San Felipe fault zone provide a record of strike-slip fault initiation at the same time as this major progradational event. Because the San Felipe anticline is related to early slip in the San Jacinto fault zone, the angular unconformity provides another link between this major progradation event and the structural driving forces (Kirby et al., 2007). Clasts reworked from the Arroyo Diablo Formation provide a clear signal of basin inversion and uplift, which itself requires a major structural reorganization at about 1.1 Ma. Recognizing a possible short lag time between earliest fault initiation and resultant erosion and progradation of coarse clastics, we assign an age of about 1.1-1.3 Ma for initiation of the San Jacinto and San Felipe fault zones (Janecke et al., in revision).

Structural Studies

The structural geology of the San Jacinto and San Felipe fault zones is complex and contains many right and left lateral strike-slip, normal and oblique-slip faults, a few reverse faults, scarps, active folds, and other structures. Our work has focused on geologic mapping of the fault zones, interpreting faults and folds, assessing the late Quaternary activity levels (when possible) of these structures, developing and refining segmentation models of the fault zones, and interpreting the cross-sectional geometry of the faults and folds using microseismic data when it is available. Our key findings are summarized below in order of (1) structural geology, (2) dextral displacements, (3) evolution and growth of the new strike-slip faults, and (4) implications of our work.

1. Structural Geology

a. The structural geology of the San Jacinto, Buck Ridge, and San Felipe fault zones is more interconnected and continuous than prior mapping showed (Fig. 7, 8 and 9). Neither the Clark nor the Buck Ridge faults dies out to the southeast, in contrast to Sharp (1972) and most subsequent studies. Instead, they intersect with other structures in the SE and are linked to one another by numerous crossing faults that strike in every direction (Belgarde, 2007; Kirby, 2005; Lutz, 2005; Steely, 2006; D. Forand, in revision; Lutz et al., 2006; Kirby et al., 2007; Steely et al., 2009). NE- and E-striking cross faults are most common.

b. The southeast parts of the Clark fault and the San Felipe fault are strongly segmented, with adjacent structural segments having different structural styles, orientations, and fault widths. The Coyote Creek fault zone is much less variable along strike and has more simple traces and fairly simple transitions between structural segments (Belgarde, 2007) (Fig. 3).

c. The Clark fault persists for an additional 25 km SE of its previously defined termination point near Palo Verde Wash (Sharp (1972), continuing SE to the NE-striking left-lateral Extra fault zone (Kirby et al., 2007 Kirby 2005; Belgarde, 2007). The Clark fault zone becomes broader and far more dispersed to the SE, and much of its significant strain is "hidden" within the mud-rich sedimentary basin deposits (Belgarde, 2007). Detailed mapping, however, clearly shows that a large amount of right lateral strain has accumulated there (Figs. 10, 11) (Kirby et al., 2007; Belgarde, 2007).

d. The Buck Ridge fault curves to the SE north of Clark Lake and becomes the Santa Rosa normal oblique-slip fault (Belgarde, 2007;Janecke and Forand, unpublished mapping). Several strands of the Santa Rosa fault connect with the Clark fault near Lute Ridge (Figs. 3, 4, 9, 10, and 11) (Belgarde and Janecke, in Belgarde, 2007).

e. Folding accommodates dextral strains and block rotation (?) at the SE end of the Clark fault zone (Fig. 14; in the last 2-2.5 km)(Kirby et al., 2007; Janecke, unpublished mapping). There is no surface connection between the SE tip of a fault within the Clark fault zone and the Extra fault. A blind structure at depth might persist to the intersection (Kirby, 2005; Janecke, unpublished mapping).

f. Strike--slip faults have "atypical" geometries in mud-rich sedimentary rocks, including ramps and flats (Figs. 10, 11, 12, 13, 14, 15, 16, 17, 18, 19) dipping "thrust-like" geometries, pitchfork structures (Fig. 19) faults that cross one another at the same structural level (Figs. 10, 12), faults that pass over (cross) and under one another at different structural levels (Figs. 15, 18), fault-parallel fault-bend folds (Fig. 15 and Steely et al., 2009), and pooch structures. These tend to distribute strain over large areas and transfer large strains to distant locations (Figs. 1, 3, 4, 10, 12, 15, 16, 17) (Kirby, 2005; Belgarde, 2007).

In general, we find that there are many linkages between adjacent dextral faults. Dozens of additional faults with trace lengths up to 25 km connect the Coyote Creek and Clark faults to one another, to adjacent faults, and likely transfer strain back and forth between them. Similar fault networks connect the San Felipe fault north to the Coyote Creek fault and south to the Earthquake Valley fault zone. It is challenging to parse this interconnected web of faults into discrete fault zones, to precisely quantify the strain in rotating blocks, damage zones, and on subsidiary structures, despite clear signs of localized dextral faults in many areas.

2. Dextral Displacements and Lifetime Slip Rates

a. The Clark fault has at least 14.4 km of right separation across Clark Valley (Sharp, 1967). New data since the field trip revises this slip up to 16.8 km (Forand, in revision) (Figs. 4 and 7). For simplicity we did not revise the present guide for this new value.

b. The Coyote Creek fault at Coyote Mountain has 3.5±1.3 km of right slip, not the ca. 6 km of prior estimates that were based on Sharp's (1967) map of the base of the Cretaceous Eastern Peninsular Ranges mylonite zone (Dorsey, 2002). The new estimate measures displacement of a distinctive and steeply dipping suite of crystalline rocks across the fault zone (Janecke et al., in revision) (Figs. 7 and 8).

c. More than 6 km of right slip on the Clark fault accrued in the Tarantula Wash fault segment on the San Felipe Hills since about 0.55 ± 0.2 Ma. This is a minimum slip rate of at least 10.2 (+6.9/-3.3) mm/yr (Kirby, 2005; Janecke et al., in revision).

d. The San Felipe fault zone is a more important Quaternary fault zone than previously recognized. It offsets planar features 4-13 km with a preferred slip estimate of 6.5 km since ~1.1 to 1.3 Ma (Steely et al., 2009; Janecke et al., in revision) (Fig. 3).

e. Using new total offsets of 17.9±1.3 km across the Clark, Buck Ridge and Coyote Creek faults and the initiation ages for the relevant fault segments between 0.8-1.3 Ma, the combined lifetime slip rate across the San Jacinto fault zone is approximately 17.8 +2.6 -2.3 mm/yr (Janecke et al., in revision) (Fig. 5). Incompletely known strains in the damage zone of the major faults and the additional 2.4 km of strain across the Clark fault increase this estimate, but are too preliminary to include here (Forand, in revision) (Fig. 7).

f, The San Felipe fault zone has a lifetime average slip rate of ~5.4 +6.9 -2.3 mm/yr that is based on its 6.5 km of slip and the range of possible displacements and ages. This exceeds the lifetime slip rate of the southern Elsinore and Coyote Creek faults (Janecke et al., in revision).

g. Overall, our data sets suggest that lifetime slip rates are fairly high (Fig. 8 and Table 2). Together the San Jacinto and San Felipe fault zones appear to have accumulated roughly half the plate rate since they formed in the early Pleistocene (17.8 + 5.4=23.2 mm/yr).

3. Evolution and Growth of New Strike-Slip Faults:

a. The faults did not emerge in their present form at 1.1-1.3 Ma. Instead, major structures like the basement-cored San Felipe anticline developed in the San Jacinto fault zone during its early history and have been deactivated, cut, and displacement during its later history (Lutz et al., 2006; Kirby et al., 2007; Steely, 2006).

b. Another example of an evolving fault zone is the San Felipe fault zone. During the first half of its existence near Sunset Wash, over 600 m of conglomerate and pebbly sandstone accumulated within the fault zone. During the second half of its history, as a contractional stepover tightened, these deposits were folded, uplifted and exhumed (Steely et al., 2009).

c. In general folding related to the dextral faults was broad and widely spaced during the early history of deformation, producing disconformities, progressive unconformities, and lateral thickness changes across many-kilometer-wide tilt panels (e.g. Fig. 15A-C). Later (after about 0.5 Ma) folding strains increased, became more localized and folds with mappable hinges are spaced roughly 750-100 m apart (Fig. 15D)(Kirby, 2005; Kirby et al., 2007; Lutz, 2005; Steely et al., 2009).

d. Despite the very young age of the fault zones (1.1 to 1.3 Ma) they have already been reorganized structurally and the main strands have shifted laterally (Kirby, 2005; Kirby et al., 2007; Lutz, 2005; Lutz et al., 2006; Steely, 2006; Steely et al., 2009; Belgarde, 2007).

4. Implications of This Work:

a. It is very unlikely that the slip rates of the San Jacinto and San Felipe fault zones were constant over their life spans because the fault zones changed their geometry and principal faults as they evolved. Models that assume steady-state behavior in such a complex fault zone (with rapidly evolving links and a complex fault mesh) are unlikely to be correct (Janecke et al., in revision.).

b. Displacements and ages of fault segments vary from place to place and therefore slip rates vary along the strike of the fault zones. Care must be taken when comparing slip rates at different time scales, from different segments, and across different faults.

c. Some fault zones have so much strain in their damage zone that it is difficult to accurately measure total displacements in their central strands. The Clark fault in the Arroyo Salada and Tarantula Wash segments display this character (Belgarde, 2007) (Figs. 10-19). We are also finding additional strain in crystalline rocks between the Coyote Creek and Clark fault at Coyote Mountain and Coyote Ridge (Forand, in revision).

Concluding Remarks

Recent and ongoing studies by our group show that the San Jacinto and San Felipe fault zones initiated at ca. 1.1-1.3 Ma, during a tectonic reorganization that profoundly changed and widened the distribution of plate-boundary strain in the southern San Andreas fault system. This tectonic event deactivated most of the West Salton detachment fault – though some parts continued to slip in the south – and quickly inverted western parts of the supradetachment basin. This drove rapid uplift and erosion of uplifting fault blocks along the San Felipe and San Jacinto fault zone and progradation of coarse alluvial and fluvial deposits (Ocotillo and Brawley formations) across the western Salton Trough, and completely changed the landscape. Another, less profound change at ~0.5-0.6 Ma caused basins that had collected the Ocotillo and Brawley formations to stop subsiding, resulting in deposition of the first of many pediment deposits, the Fonts Point Sandstone, over a large area. This change initiated the current phase of fault-zone deformation, uplift and erosion that has been active over the past ~ 500 kyrs.

We conclude that slip rates in these fault zones likely vary along the strike, and probably varied significantly over time. The geologic lifetime rate that we calculate for the San Jacinto fault zone – approximately 17.8 +2.6 -2.3 mm/yr – is closer to rates derived from GPS and InSAR inversions than those based on paleoseismic studies and dating of offset Quaternary to Holocene geomorphic features (Table 1 and Le et al., in press). We suggest that slip rates determined from paleoseismic and neotectonic methods may be incomplete in settings, like the southeast half of the San Jacinto fault zone, where large amounts of strain are taken up outside the main central fault strands. The broad distribution of strain in the damage zones of major faults may hinder attempts to reconcile different timescales of slip rates in this and other active fault zones.

PART II: ROAD LOG

Stop 1: Borrego Springs Airport (33° 15.447' N, 116° 19.532' W)

Overview and introduction.

(NOTE: we may drive a short north on a dirt road located about 0.4 mi. west of the airport, in order to get a better view). From here we can see the SW edge of Coyote Mountain (Fig. 20) and the SW side of the Santa Rosa Mountains (Fig. 21). Figure 2 shows the points of interest on the north edge of San Isidro Mountains (likely not in view), SW edge of Coyote Mountain (CM) and the SW part of the Santa Rosa Mountains. Look for the white marble-rich intervals between the biotite and hornblende-bearing tonalite to the west and the dark weathering biotite-rich migmatite to the east. These units correlate across the fault zones. Table 2 shows the displacement estimates from this analysis as well as the lifetime slip rates. Figures 1 to 10 also pertain to this stop.

Drive NE from stop 1 along the Borrego-Salton Seaway highway toward Salton City. About 8.5 miles from the airport is Lute Ridge to the north. This prominent hill has an escarpment on its far NE side that coincides with the main trace of the Clark fault. Numerous smaller scarps displace the pediment that lies in angular unconformity on folded older Quaternary conglomerate. Figure 10 shows a new interpretation of the uplift in Lute Ridge and the folding in low hills a few kilometers to the NW. We interpret this area as preserving extensional and contractional steps between subparallel strands of the dextral Clark fault zone. See Belgarde (2007) for details.

Continue driving east to the turn-off into Coachwhip Canyon on the left/north side of the road. The turn off is not all that well marked. Drive about 0.5 miles to stop 2.

STOP 2: Coachwhip Canyon (33° 17.428' N, 116° 8.949' W). Figs. 9, 10, 12, 13.

Park and examine the multiple strands of the Clark fault that parallel bedding in pebbly sandstone of the fine Canebrake and coarse Olla formations. The beds dip south and the faults do too. Microseismicity shows that at least one strand of the Clark fault about 0.5 km farther up the canyon dips steeply to the SE at depth (Fig. 17) (Belgarde, 2007). This requires a bend in the fault plane and reversal of the dip direction. Notice the well-developed clay gouge in excellent exposures of the fault. Other parts of the fault have almost no gouge and could be mistaken for intact bedding planes, particularly in areas of typical exposure. This exposure of the fault is along strike of a scarp in late Pleistocene pediment deposits. Refer to figures 5, 6, 11, 12 and 13. OSL ages range from 21.72 ± 1.19 to 62.26 ± 4.05 ka in these pediment deposits (Rittenour, Janecke and Belgarde, unpublished; Janecke et al, in revision).

Coachwhip Canyon illustrates the character of the Clark fault zone in moderately well-lithified units like the Canebrake Formation. Faults dominate in these settings. Where mud becomes a major constituent, folding becomes much more common in the fault zone and the Clark fault broadens (Fig. 15). The Clark fault zone is up to 18 km wide in map view in the Arroyo Salada and Tarantula Wash segments (Belgarde, 2007) (Fig. 13).

Exit Coachwhip Canyon. Drive east on the paved highway to the turn-around and pull-out at 33° 17.044'N 116° 7.788'W. This is about 1.5 miles to the east. The scarp that coincides with the fault exposed at stop 2 is located about 2/3 of the way from Coachwhip Canyon to the

turn-around. On the way to the turn-around notice the numerous SW-facing fault scarps on the pediment surface. Each of these scarps is along strike of a bedding parallel fault strand of the Clark fault zone in Coachwhip Canyon. We dated this pediment deposit in an exposure about 1 km SSE of the turn around. From the turn-around it is about 1 km SSE to the location of a dated portion of this pediment surface. A fine-grained sand-bearing bed near the base of the pediment deposit produced a late Pleistocene OSL age of 30.71 ±2.34 ka OSL age (Rittenour, Belgarde, and Janecke, unpublished data; Janecke et al, in revision).

Turn around and drive back to Arroyo Salada. Turn south opposite Coachwhip Canyon and drive ESE down Arroyo Salada, past the primitive campground, for about 3.5 miles. Two wheel drive is adequate unless it has rained.

Stop 3a: Clark fault zone in Arroyo Salada (33° 15.363' N, 116° 6.559' W)

A wide steep fault zone is exposed in the west wall of Arroyo Salada (Belgarde, 2007). This is one of the main strands of the Clark fault zone in the Arroyo Salada segment. Note how the main fault planes parallel bedding planes and are very thin. Prior to a fortuitous rock fall, this fault zone looked like it was intact stratigraphic section. Slickenlines range in direction and include an important population of strike-slip slickenlines. If stop 3a is poorly exposed due to weathering, continue SE to stop 3b. This stop further illustrates the hidden faulting in the sedimentary units. This fault was mapped as a minor thrust fault by Jarg Pettinga but the horizontal slickenlines show that it is instead a major central strand of the Clark fault zone. At least half a dozen similar strands parallel this one, and there is significant deformation dispersed across a region ~18 km wide perpendicular to the fault zone at this spot (Figs. 10, 11, 12, 14, and 16). The low pediment is not cut by the fault at this stop.

Stop 3b: alternate to stop 3a (33° 14.305' N, 116° 5.804' W)

If stop 3a has been covered over by gully wash or we are running ahead of time, continue to stop 3b another 1.7 to 2 miles to the SSE. Drive SE past the turn-off to 17 Palms and turn right into a narrow track leading to Tule Wash. Whenever the road splits turn left or follow any signs to Tule Wash, and drive to the fault exposed at stop 3b. This smaller fault has a NE strike and is a left-oblique strike-slip fault. It is exciting because it is one of a large population of NE– to E-striking left-oblique faults that dominate the SW 40% of the Clark fault's damage zone in the Arroyo Salada and Tarantula Wash fault segment (Fig. 12). The deep structure beneath these left-oblique faults is completely different, however, and consists of a 6-13 km deep planar fault, which is called the Tule Wash fault (Belgarde, 2007) (Fig. 17 and 18). The Tule Wash fault dips steeply NE and passes beneath the shallow and subvertical NE-striking faults exposed at the surface. A decollement surface must separate the incompatible structures at the shallow and deep levels. We envision a left-oblique fault array on an "overpass" and a steeply NE-dipping dextral fault on an "underpass" (Janecke and Belgarde, 2007, 2008) (Figs. 12, 17, 18). Decollements and pitchfork fault structures, like those modeled by Le Guerroué and Cobbold in Figure 19 E, may facilitate this behavior.

Crossing strike-slip faults also interfere with one another at the same structural level in other parts of the field area (Fig. 11). Mutual interference and mutual bending developed in these situations.

Turn around and return to pavement. Drive west on the Borrego-Salton Seaway Highway for about 5.5 miles. Turn SW (left) into Fonts Wash and follow the signs and track up

to Fonts Point in the south.

Stop 4: Fonts Point (33° 15.454' N, 116° 13.958' W)

The view looking south from Fonts Point provides a breath-taking vista of the Borrego and Ocotillo formations exposed in the southern Borrego Badlands, as well as other features including Borrego Mountain which is cut by strands of the Coyote Creek fault, the complexly faulted eastern of the Peninsular Ranges, and low-lying sedimentary rocks of the western Salton Trough. Here we are standing at the top of a precipitous erosional escarpment that is currently retreating to the north as a result of ongoing uplift and erosion in the Borrego Badlands. Figure 2.

The Ocotillo Formation is exposed beneath and east of Fonts Point in the erosional escarpment. Using magnetostratigraphy calibrated with the 0.76-Ma Bishop Ash, the sharp base of the Ocotillo Formation was dated at 1.05 ± 0.03 Ma (Lutz, 2005; Lutz et al., 2006). This contact records abrupt expansion of alluvial-fan and fluvial systems that prograded rapidly into and across the former Borrego lake depocenter at this time. Paleocurrent data show that coarse sediment entered the basin from multiple newly emergent sources located south and SW (Vallecito Mts.), west and NW (San Ysidro Mts.), north (Coyote Mt.), and NE (southern Santa Rosa Mts.) of the Borrego Badlands depocenter (Lutz et al., 2006). A systematic up-section increase in C-suite sandstone clasts recycled from the Arroyo Diablo Formation provides evidence for uplift and exhumation of the former hangingwall basin of the WSDF (ibid). Isopach and facies patterns record syn-basinal titling to the NE in response to growth of the San Felipe anticline and oblique slip on the Clark fault (ibid). Based on this and companion studies by Kirby et al. (2007) and Steely et al. (2009), we conclude that rapid progradation of the Ocotillo and Brawley formations across the western Salton Trough was driven by a dramatic increase in sediment flux from the eastern Peninsular Ranges at ~1.1 Ma. This marks a major, tectonically controlled basin reorganization that resulted from initiation of the San Jacinto and San Felipe fault zones and related onset of uplift and erosion in the former hanging-wall of the Late Cenozoic West Salton detachment fault.

Stop 5: Overview of San Felipe fault zone (33° 7.962' N, 116° 17.264' W)

This stop (which is based on Steely, 2006 and Steely et al., 2009) illustrates the typical relationship between Pleistocene to Recent strike slip faults and Ocotillo Formation. We are located within a double contractional stepover of the San Felipe fault zone. This relatively unknown dextral strike slip fault reaches from the NW Elsinore fault to the SE part of the San Jacinto fault zone. It is about 60 km long from end to end. In the Yaqui Ridge area there is a cross-cutting relationships between the San Felipe fault zone and the older West Salton detachment fault, as well as syntectonic deposits shed from the nascent San Felipe fault zone. Structurally, the San Felipe fault zone steps left from the large fault on the N side of the Fish Creek Mountains and Vallecito Mountains (the Fish Creek Mountains fault) to the San Felipe fault. The San Felipe fault is south of here under San Felipe Wash and at the base of Yaqui Ridge. A small fault called the Sunset fault is parallel to these two larger structures and lies a couple hundred meters NE of our stop. Slip steps from the Fish Creek Mountains fault to the Sunset fault and then SW to the San Felipe fault. A thick section of folded and faulted conglomerate is north of the Sunset fault, whereas the folded West Salton detachment, mylonite and other crystalline rocks lie south of the Sunset fault. See Steely et al. (2009) for an overly

long structural discussion of this stepover.

Our purpose today is to illustrate the stratigraphic and sedimentary record of initial slip n the San Felipe fault zone. The conglomerates that we can see from here, on the NE side of Sunset Wash, were correlated to the Pliocene Canebrake Conglomerate by Dibblee (1954). Detailed mapping and analysis by Steely et al. (2009) shows that this conglomerate correlates instead to the early to middle Pleistocene Ocotillo Formation. The Canebrake is derived from the footwall of the West Salton detachment fault (Axen and Fletcher, 1998; Kairouz, 2005; Steely, 2006). The conglomerate along Sunset Wash does not contain a single clast of mylonite derived from the footwall of the detachment fault, despite being located as little a 300 m NE of the detachment fault. Its provenance was exclusively in the hanging wall of the detachment fault and most of the sediment was shed from displaced and uplifted plutonic rocks immediately SW of the Sunset fault (See figures in Steely et al., 2009). Paleocurrents show dispersal to the NE, grain size decreases in that direction, and the composition and grain size are perfectly concordant with those in the Ocotillo formation nearby. Boulders up to 4 m across near the Sunset fault attest to active tectonism within the San Felipe fault zone and across the Sunset fault during deposition of the conglomerate. An angular unconformity, missing units beneath the Ocotillo Formation about a km SE of here, and the presence of recycled sandstone clasts derived from the Pliocene Arroyo Diablo Formation further support our interpretation.

Very similar relationships exist adjacent to the San Jacinto fault zone, and show that the Ocotillo formation, and its finer lateral equivalent, the Brawley Formation, were deposited in a new sedimentary basin ringed by brand new dextral oblique strike slip faults. The Ocotillo formation thickens by a factor of ~2 NE toward the Clark fault from a condensed section near Font's Point (Stop 4)(Lutz et al., 2007). The Ocotillo Formation coarsens in that direction and contains distinctive clasts shed from the NE side of the Clark fault. Paleocurrents indicate southward flow. Westward thickening and coarsening, and eastward paleocurrent show that the East Coyote Mountain fault was an active structure within the San Jacinto fault zone starting about 1.05 Ma (Lutz et al., 2006). A disconformity and angular unconformity separate the Ocotillo and Brawley formation from the underlying basin fill, and mark the change from syndetachment to syn-strike slip deposition.

Concluding remarks

Many lines of evidence now show that the San Felipe and San Jacinto fault zone are early Pleistocene dextral faults with high lifetime slip rates. Refined and new displacement estimates, combined with magnetostratigraphic dating of the Borrego/Ocotillo contact are the main constraint on this. In addition, the San Jacinto fault zone is far more complex and broad than generally thought. This is especially true where the fault deforms mud-rich sedimentary rocks but dispersed faults are also developed in the crystalline damage zone adjacent to the central part of the fault zone. We believe that this dispersed deformation partly explains the lower slip rates determined in neotectonic studies (e.g. Le et al., in press) when compared to slip rates inverted from GPS data and calculated using offset bedrock features (Fig. 8, tables 1 and 2)(Janecke et al., in revision). Refer to part 1 for references and figures.

REFERENCES

Albright, L.B., 1999, Magnetostratigraphy and biochronology of the San Timoteo Badlands, southern California, with implications for local Pliocene-Pleistocene tectonic and depositional patterns: Geological Society of America Bulletin, v. 111, p. 1265-1293.

Anderson, G., Agnew, D.C., and Johnson, H.O., 2003, Salton Trough regional deformation estimated from combined trilateration and survey-mode GPS data: Bulletin of the Seismological Society of America, v. 93, p. 2402-2414.

Axen, G.J., and Fletcher, J.M., 1998, Late Miocene-Pleistocene extensional faulting, northern Gulf of California, Mexico and Salton Trough, California. International Geology Review v. 40, p. 217-244.

Becker, T.W., Hardebeck, J.L., and Anderson, G., 2005, Constraints on fault slip rates of the southern California plate boundary from GPS velocity and stress inversions: Geophysical Journal International, v. 160, p. 634–650 doi: 10.1111/j.1365-246X.2004.02528.x

Belgarde, B.E., 2007, Structural characterization of the three southeast segments of the Clark fault, Salton Trough, California [M.S thesis]: Utah State University: 4 plates, map scale 1:24,000, 216 p.

Bennett, R. A., Rodi, W., and Reilinger, R. E., 1996, Global Positioning System constraints on fault slip rates in southern California and northern Baja, Mexico: Journal of Geophysical Research,v. 101, p. 21,943–21,960.

Blisniuk, K., Rockwell, T., Owen, L.A., Oskin, M., Lewis A. Owen, Michael Oskin, Lippincott, C., Caffee, M.W., Dortch, J., in press, Late Quaternary slip rate gradient defined using high-resolution topography and 10Be dating of offset landforms on the southern San Jacinto Fault zone, California: Journal of Geophysical Research.

Dibblee, T.W., Jr., 1954, Geology of the Imperial Valley region, California. Geology of Southern California, California Division of Mines Bulletin 170, p. 21-28.

Dibblee, T.W., 1984, Stratigraphy and tectonics of the San Felipe Hills, Borrego Badlands, Superstition Hills, and vicinity. In Rigsby, C. A. (ed.), The Imperial Basin - Tectonics, Sedimentation, and Thermal Aspects. Los Angeles, California, Pacific Section S.E.P.M., p. 31-44.

Dibblee. T.W., Jr., 1996, Stratigraphy and tectonics of the Vallecito-Fish Creek Mountains, Vallecito Badlands, Coyote Mountains and Yuha Desert, southwestern Imperial basin, California, in Abbott, P.L., and Seymore, D. C., eds., Sturzstroms and detachment faults, Anza-Borrego Desert State Park, California: South Coast Geological Society, Santa Ana, California, Annual Field Trip Guidebook 24, p. 59-79.

Dorsey, R.J., 2002, Stratigraphic record of Pleistocene initiation and slip on the Coyote Creek fault, lower Coyote Creek, southern California, In Barth, A., ed., Contributions to Crustal Evolution of the Southwestern United States: Geological Society of America Special Paper 365, p. 251–269.

Dorsey, R.J., 2006, Stratigraphy, tectonics, and basin evolution in the Anza-Borrego Desert region. In: Jefferson, G.T. and Lindsay, L.E. (eds.) Fossil Treasures of Anza-Borrego Desert. Sunbelt Publications, San Diego, CA, p. 89-104.

Dorsey, R. J., Fluette, A., McDougall,. K. A., Housen, B. A., Janecke, S. U., Axen, G. A., and Shirvell, C. R., 2007, Chronology of Miocene-Pliocene deposits at Split Mountain Gorge, southern California: A record of regional tectonics and Colorado River evolution: Geology, v. 35, p. 57-60.

Fay, N.P., and Humphreys E.D., 2006, Dynamics of the Salton block: Absolute fault strength and crust-mantle coupling in Southern California. Geology, v. 34, p. 261-264.

Fialko, Y., 2006, Interseismic strain accumulation and the earthquake potential on the southern San Andreas fault System: Nature v. 441, p. 968-971.

Forand, D., in revision, Structural geology of two crystalline damage zones, southern California [MS thesis]: Utah State University.

Hill, R.I., 1984, Petrology and petrogenesis of batholithic rocks, San Jacinto Mountains, southern California: Pasadena, California Institute of Technology [Ph.D. dissertation]: 660 p.

Hudnut, K., L. Seeber, and T. Rockwell, 1989, Slip on the Elmore Ranch fault during the past 330 years and its relation to slip on the Superstition Hills fault: Bulletin of the Seismological Society of America, v. 79, p. 330–341.

Janecke, S.U., Dorsey, R.J., Steely, A.N., Kirby, Andrew Lutz, S.M., Housen, B.A., Belgarde, B., and Langenheim, V., Rittenour, T. and Forand, D., in revision, High Geologic Slip Rates since Early Pleistocene initiation of the San Jacinto and San Felipe Fault Zones in the San Andreas fault system: Southern California, USA: GSA Special Paper.

Janecke, S.U., Belgarde, B.E., 2007, The width of dextral fault zones and shallow decollements of the San Jacinto fault zone, southern California: Annual meeting of the Southern California Earthquake Center, Palm Springs, CA, v. 17. http://www.scec.org/meetings/2007am/index.html

Janecke, S.U., and Belgarde, B.E., 2008, Detecting hidden, high-slip rate faults: S. San Jacinto fault zone; Final Report for NEHRP Grant 06HQGR0031, 96 p. http://earthquake.usgs.gov/research/external/research.php?yearID=2006&pi=janecke&regionID=&award=&keyword=&submit=Find+Projects

Janecke, S.U., Steely, A.N., and Evans, J.P., 2008, Seismic Slip on an Oblique Detachment Fault at Low Angle: Eos Trans. AGU, 89 (53), Fall Meet. Suppl., Abstract T53F-06.

Janecke, S.U., Kirby, S.M., Langenheim, V.E., Housen, B.A., Dorsey, R.J., Crippen, R.E., Blom, R.G., 2004, Kinematics and evolutions of the San Jacinto fault zone in the Salton Trough: Progress Report from the San Felipe Hills area: Geological Society of America Abstracts with Programs, v. 37, no. 5, p. 317. http://gsa.confex.com/gsa/2004AM/finalprogram/abstract_78180.htm

Jennings, C.W., 1994, Fault activity map of California and adjacent areas, with locations and ages of recent volcanic eruptions: California Division of Mines and Geology, Geologic Data Map No. 6, map scale 1:750,000.

Jennings, C.W., compiler, 1977, Geologic map of California: California Division of Mines and Geology Geologic Data Map 2, scale 1:750,000.

Kairouz, M.E., 2005, Geology of the Whale Peak Region of the Vallecito Mountains: Emphasis on the Kinematics and Timing of the West Salton Detachment fault, Southern California, [M.S. Thesis]: University of California, Los Angeles. 156 p.

Kendrick, K.J., Morton, D.M., Wells, S.G., and Simpson, R.W., 2002, Spatial and Temporal Deformation along the Northern San Jacinto Fault, Southern California: Implications for Slip Rates: Bulletin of the Seismological Society of America, v. 92, p. 2782 - 2802.

Kennedy, M.P., 2000, Preliminary geologic map of the Pechanga 7.5' quadrangle, San Diego and Riverside Counties, California. http://www.consrv.ca.gov/cgs/rghm/rgm/preliminary_geologic_maps.htm

Kennedy, M.P., 2003, Preliminary geologic map of the Vail Lake 7.5' quadrangle, San Diego and Riverside Counties, California. http://www.consrv.ca.gov/cgs/rghm/rgm/preliminary_geologic_maps.htm

Kennedy, M.P., and Morton, D.M., 2003, Preliminary geologic map of the Murrieta 7.5' quadrangle, Riverside County, California. U.S. Geological Survey Open-File Report 03-189, 17 p., scale 1:24,000, http://geopbs.wr.usgs.gov/open-file/of03-189/.

King, N.E., and Savage, J.C., 1983, Strain-rate profile across the Elsinore, San Jacinto and the San Andreas faults near Palm Springs, California, 1973-81: Geophysical Research Letters, v. 10, p. 55-37.

Kirby, S.M., 2005, The Quaternary tectonic and structural evolution of the San Felipe Hills, California, [M.S. Thesis]: Logan, Utah State University, 182 p.

Kirby, S.M., Janecke, S.U., Dorsey, R.J., Housen, B.A., McDougall, K., Langenheim, V., and Steely, A. Jan 2007, Pleistocene Brawley and Ocotillo formations: Evidence for initial strike-slip deformation along the San Felipe and San Jacinto fault zones, California: Journal of Geology, v. 115, p. 43-62.

Lutz, A.T., 2005, Tectonic controls on Pleistocene basin evolution in the central San Jacinto fault zone, southern California, [M.S. thesis]: Eugene, University of Oregon, 136 p.

Lutz, A.T., Dorsey, R.J., Housen, B.A., and Janecke, S.U., 2006, Stratigraphic record of Pleistocene faulting and basin evolution in the Borrego Badlands, San Jacinto fault zone, southern California: Geological Society of America Bulletin, v. 118, p. 1377-1397; DOI: 10.1130/B25946.1.

Magistrale, H., 2002, The relation of the southern San Jacinto fault zone to the Imperial and Cerro Prieto faults. Special Paper 365: Contributions to Crustal Evolution of the Southwestern United States: v. 365, p. 271–278.

Matti, J.C., and Morton D.M., 1993, Paleogeographic evolution of the San Andreas Fault in Southern California: A reconstruction based on a new cross-fault correlation. In: Powell, R.E., Weldon, R J., and Matti, J.C. Eds., The San Andreas Fault System: Displacement, Palinspastic Reconstruction, and Geologic Evolution. Geological Society of America Memoir v. 178, p. 107-159.

McCaffrey R., 2005, Block kinematics of the Pacific-North America plate boundary in the southwestern United States from inversion of GPS, seismological, and geologic data: Journal of Geophysical Research, v. 110, B07401, doi:10.1029/2004JB003307.

Meade, B. J., and B. H. Hager, 2005, Block models of crustal motion in southern California constrained by GPS measurements: Journal of Geophysical Research, v. 110, B03403, doi:10.1029/2004JB003209.

Meisling, R., and Weldon, K., 1989, Late Cenozoic tectonics of the northwestern San Bernardino Mountains, Southern California: Geological Society of America Bulletin, v. 101, p. 106-128.

Morton, D.M., 1999, Preliminary digital geologic map of the Santa Ana 30'x60' quadrangle, southern California, version 1.0. : U.S. Geological Survey Open-File Report 99-172, U.S. Geological Survey, California.

Morton, D.M., and Matti, J.C., 1993, Extension and contraction in an evolving divergent strike-slip fault complex: the San Andreas and San Jacinto fault zones at their convergence in Southern California, in Powell, R.E., Weldon, R.J., and Matti, J.C., eds., The San Andreas fault system: displacement, palinspastic reconstruction, and geologic evolution: Geological Society of America Memoir v. 178, p. 217-230.

Morton, D.M., and Kennedy, M.P., 2003, Geologic Map of the Bachelor Mountain 7.5' Quadrangle, Riverside County, California: U.S. Geological Survey Open-File Report 03-103.

Rockwell, T., Loughman, C., and Merifield, P., 1990, Late Quaternary rate of slip along the San Jacinto fault zone near Anza, Southern California: Journal of Geophysical Research, v. 95, p. 8593-8605.

Rockwell, T.K., Seitz, G., Dawson, T., and Young, J, 2006, The long record of San Jacinto fault paleoearthquakes at Hog Lake: Implications for regional patterns of strain release in the southern San Andreas fault system: Seismological Research Letters, v. 77, p. 270.

Rogers, T.H., 1965, Santa Ana sheet: California Division of Mines and Geology Geologic Map of California, scale, 1:250,000.

Sanders, C.O., 1989, Fault segmentation and earthquake occurrence in the strike-slip San Jacinto fault zone, California. In: Schwartz, D. P.; Sibson, R. H. (eds.) Proceedings of Conference XLV; a workshop on Fault segmentation and controls of rupture initiation and termination, U. S. Geological Survey Open-File Report OF 89-0315, p. 324-349.

Savage, J.C., and W.H. Prescott, 1973, Precision of Geodolite distance measurements for determining fault movements: Journal of Geophysical Research, v. 78, p. 6001–6008.

Savage, J.C., and Prescott, W.H., 1976, Strain accumulation on the San Jacinto Fault near Riverside, California: Bulletin of the Seismological Society of America, v. 66, p. 1749-1754.

Savage, J.C., Prescott, W.H., Lisowski, M., and King, N., 1979, Deformation across the Salton Trough, California 1973-1977: Journal of Geophysical Research, v. 84, p. 3069-3079.

Sharp, R.V., 1967, San Jacinto fault zone in the Peninsular Ranges of Southern California: Geological Society of America Bulletin, v. 78, p. 705-729.

Sharp, R.V., 1972, Map showing recently active breaks along the San Jacinto fault zone between the San Bernardino area and Borrego Valley, California: U. S. Geological Survey Miscellaneous Geologic Investigations Map 1-675, scale 1:24,000, 3 sheets.

Sharp, R.V., 1975, En echelon fault patterns of the San Jacinto Fault zone. In: Crowell, J.C. (ed.) San Andreas Fault in southern California; a guide to San Andreas Fault from Mexico to Carrizo Plain: Special Report - California Division of Mines and Geology, n. 118, p. 147-152.

Sharp, R.V., 1979, Some characteristics of the eastern Peninsular Ranges mylonite zone: Open-File Report - U. S. Geological Survey, Report: OF 79-1239, pp. 258-267.

Sharp, R.V., 1981, Variable rates of late Quaternary strike slip on the San Jacinto fault zone, Southern California: Journal of Geophysical Research, v. 86, p. 1754-1762

Shearer, P., Hauksson, E. and Lin, G., 2005, Southern California hypocenter relocation with waveform cross-correlation; Part 2, Results using source-specific station terms and cluster analysis: Bulletin of the Seismological Society of America, v. 95, p. 904-915.

Steely, A.N., 2006, The evolution from late Miocene west Salton detachment faulting to cross-cutting oblique strike-slip faults in the southwest Salton Trough, California [M.S thesis]: Utah State University, 253 p. 3 plates. Scale 1:24,000.

Steely, A.N., Janecke, S.U., Axen, G.J., Dorsey, R.J., 2009, Pleistocene reorganization of the southern San Andreas fault system: Initiation and structures of the San Felipe fault zone: Geological Society of America Bulletin, v. 121, p. 663–687; doi: 10.1130/B26239.1.

Weldon, R.J., Meisling, K.E., and Alexander, J., 1993, A Speculative history of the San Andreas fault in the central Transverse Ranges, in, Powell, R.E., Weldon, R.J., and Matti, J. eds., The San Andreas fault system; displacement, palinspastic reconstruction, and geologic evolution: Geological Society of America Memoir 178, p. 161-178.

Winker, C.D., and Kidwell, S.M., 1996, Stratigraphy of a marine rift basin: Neogene of the western Salton Trough, California. In Abbott, P.L., and Cooper, J.D., (eds.), Field conference guidebook and volume for the annual convention, San Diego, California, May, 1996, Bakersfield, California, Pacific Section: American Association of Petroleum Geologist, p. 295-336.

Table 1. Summary of slip rates across the San Jacinto fault zone (From Janecke et al., in prep.)

Author (in chronological order)	Method	Rate for SJFZ	Rate for SAF	Time scale	Comments
Coolidge and Whitten, 1956 As cited in Sharp, 1967	geodetic network Very long baseline	24 mm/yr¥	ND	Short	
Sharp, 1967	Geologic	25 mm/yr	ND	~1 Ma	
Savage and Prescott, 1976	geodetic network	25 mm/yr¥	ND	6 yrs	
Savage et al., 1979	Long baseline	17±9 mm/yr¥	25±8 mm/yr	4 yrs	
Sharp, 1981	paleoseismology	10±2 mm/yr 8-12 mm/yr	ND	since 0.73 Ma	Lowest rate from paleoseismic or neotectonic study
King and Savage, 1983	Long baseline	(SJFZ=88% of SAF) 21.9 mm/yr#	(SJFZ=88% of SAF) 25 mm/yr#	8 yrs	
Rockwell et al., 1990	Paleoseismology /neotectonic	10±2 mm/yr 8-12 mm/yr is preferred, 6-23 mm/yr is the total range of results	ND	50 kyr	
Morton and Matti, 1993	Geologic	25-30 km/1.5m.y. 17.4-20 mm/yr		1.4 Ma	
Matti and Morton, 1993	Geologic	25-30 km/1.2 m.y. 20.1 to 25 mm/yr		1.2 Ma	
Bennett et al., 1996	GPS	9±2 mm/yr	23±2 mm/yr	15 yrs	Lowest rate from GPS analysis
Kendrick et al., 2002	neotectonics	> 20 mm/yr			
Anderson et al., 2003	GPS	SJFZ>=SAF ≥19.5 mm/yr#	SJFZ>=SAF ≤ 19.5 mm/yr#	15 yrs	Highest rate from GPS analysis
McCaffrey, 2005	GPS	13.5 mm/yr	25.3 mm/yr	15 yrs	
Meade and Hager, 2005	GPS block model	11.9±1.2 mm/yr	23.3 ± 0.5	15 years	
Fay and Humphreys, 2005	GPS	14.5 ±0.8 mm/yr	22.3±0.7 mm/yr	15 yrs	
Becker et al., 2005	GPS plus stress inversion	15.3±11 14.5±9	23±8 mm/yr 22.9±8 mm/yr	15 yrs	
Rockwell et al., 2006*	paleoseismology	>16 mm/yr	ND	4 kyr	Highest rate from paleoseismic or neotectonic study, but this rate could be in error (T. Rockwell, pers. comm., 2007)
Fialko, 2006	InSAR plus GPS	20±1 mm/yr	25± 3 mm/yr	8 yrs-InSAR, 20 yrs GPS	
This study	Lifetime geologic slip rate	17.8 +2.6 -2.3 mm/yr	ND	0.8 to 1.3 Ma	

¥Linear slip rate was calculated from the rotational strain rate reported in this article

*Site crosses just one of several strands that were active in the Quaternary (Janecke, unpublished data) and therefore may capture less than the full slip rate. The earthquakes clustered in time, however, making the rate higher than average (Rockwell, oral comm., 2006).

We calculated a rate of slip by assuming a combined slip rate of 38.9 mm/yr across both the San Jacinto and southern San Andreas fault. This value is the average of all the rates in this table.

Table 2A Lifetime slip rates across the San Jacinto fault zone

Fault zone	Fault within fault zone	Structural segment (s) along the fault (see fig. 3b)	Slip estimate (since ~0.5 Ma)	Offset feature	Estimated age of initiation of the fault segment	Lifetime slip rate (interval rate)	Source of data used to calculate the slip rate
San Jacinto	Clark (folding in the damage zone was not included)	Santa Rosa and Arroyo Salada	14.4 km* no error was given in Sharp (1967)	Succession of tonalite, marble, migmatite, mylonite	1.0 to 1.1 Ma	13.7 +0.7 -0.6 mm/yr	Sharp, 1967; Lutz et al., 2006
San - Jacinto	Coyote Creek (folding in damage zone was not included)	Coyote Ridge	3.5±1.3 km *	Tonalite, marble, migmatite, mylonite	0.9 to 0.8 Ma	4.1 +1.9 -1.7 mm/yr	This study, updated from data in Sharp, 1967; Dorsey 2002
Total slip rate across the San Jacinto fault zone in its lifetime					**SUM**	**17.8 +2.6 -2.3 mm/yr**	**This study**

Table 2B. ~0.5 Ma slip rates across the San Jacinto fault zone

Fault zone	Fault within fault zone	Structural segment (s) along the fault (see fig. 3b)	Slip estimate (since ~0.5 Ma)	Offset feature	Estimated age of initiation of the fault segment	Lifetime slip rate (interval rate)	Source of data used to calculate the slip rate
San Jacinto	Clark	San Felipe Hills	(5.6 ±0.4 km)†	Calculated from amount of N-S shortening in Pliocene-Pleistocene sedimentary rocks	<~0.55±0.2 Ma,	≥10.2 + 6.9 -3.3 mm/yr	Kirby, 2005; Janecke et al., 2005; this study
San Jacinto	Coyote Creek	Borrego Mountain and Borrego Badlands	1-2 km†	North-dipping marker bed near contact between Olla and Diablo formations	< 0.6 Ma	2.5 ± 0.8 mm/yr	Steely, 2006, this study
Minimum slip rate across the San Jacinto fault zone since ~0.5 to 0.6 Ma					**SUM**	**(≥12.7 + 7.7 -4.1 mm/yr)**	**This study**

Table 2C Lifetime slip rate across parts of the San Felipe fault zone

Fault zone	Fault within fault zone	Structural segment (s) along the fault (see fig. 3b)	Slip estimate (since ~ 0.5 Ma)	Offset feature	Estimated age of initiation of the fault segment	Lifetime slip rate (interval rate)	Source of data used to calculate the slip rate
San Felipe	Sunset	Sunset	<2.5 km	Provenance link between displaced Ocotillo formation and its possible source area in the La Posta pluton	1.3 to 1.1 Ma	<2.1 ± 0.2 mm/yr	Steely, 2006
San Felipe	San Felipe	Pinyon Mountain and Mescal Bajada	4 to 13.5 km* 6.5 km preferred‡	West Salton detachment fault and base of the Eastern Peninsular Ranges mylonite zone	~1.3 to 1.1 Ma	~5.4 +6.9 -2.3 mm/yr ()	Steely, 2006, and this study

* displacement of crystalline markers or preexisting structural feature

† displacement is based on deformed or offset Pliocene-Pleistocene sedimentary rocks

‡Three separate methods were used to estimate the right slip and ~6.5 km is the overlap between methods. From Janecke et al., in prep.

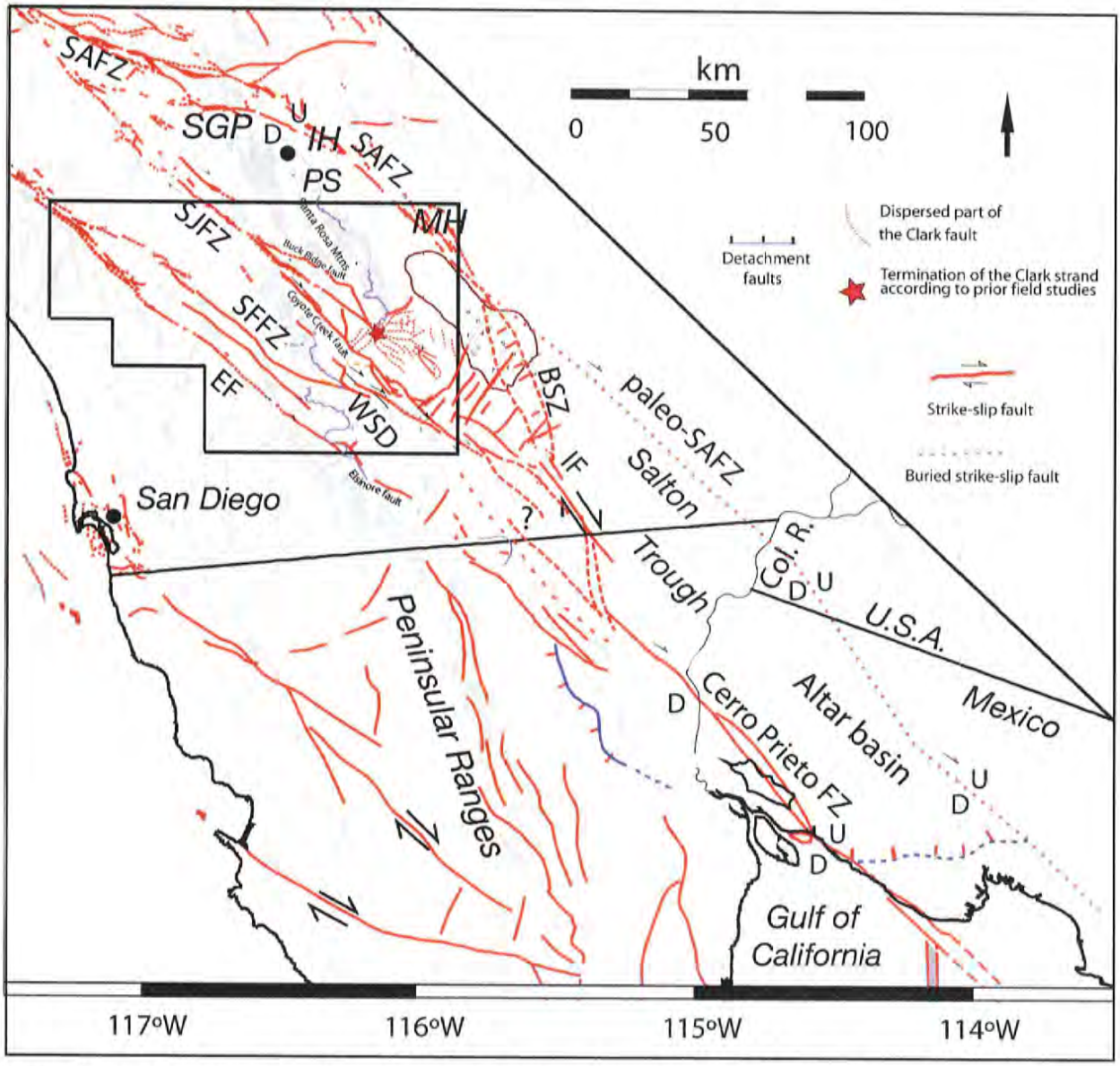

Figure 1. Tectonic overview of southern California and northwestern Mexico. This regional fault map shows how the San Jacinto fault and San Felipe fault link with the southernmost San Andreas fault, Brawley seismic zone, and Imperial faults farther to the southeast. A Cretaceous mylonite zone is offset about 15km across the Clark fault south of the Santa Rosa Mountains yet the fault was thought to terminate at the star by most prior workers. Modified from many sources including Jennings, 1977, 1994; Janecke et al., 2004; Kirby, 2005; Hudnut et al., 1989. Axen and Fletcher, 1998, Steely, 2006, Lutz, 2005, Kirby 2005; Belgarde, 2007; Janecke, unpublished mapping. San Felipe fault zone (SFFZ); SAFZ-San Andreas fault zone; SJFZ-San Jacinto fault zone; EF-Elsinore fault; BSZ-Brawley Seismic Zone; IF-Imperial fault; SJFZ-San Jacinto fault zone. SGP, San Gorgonio Pass; PS, Palm Springs. Oblique-slip detachment faults are in blue including the WSD-West Salton detachment fault. Fault locations are from Jennings (1977) and Axen and Fletcher (1998).

Figure 2. Map showing the locations of the stop on Day 2. Stop 4 and 5 are best visited late in the day shortly before sunset.

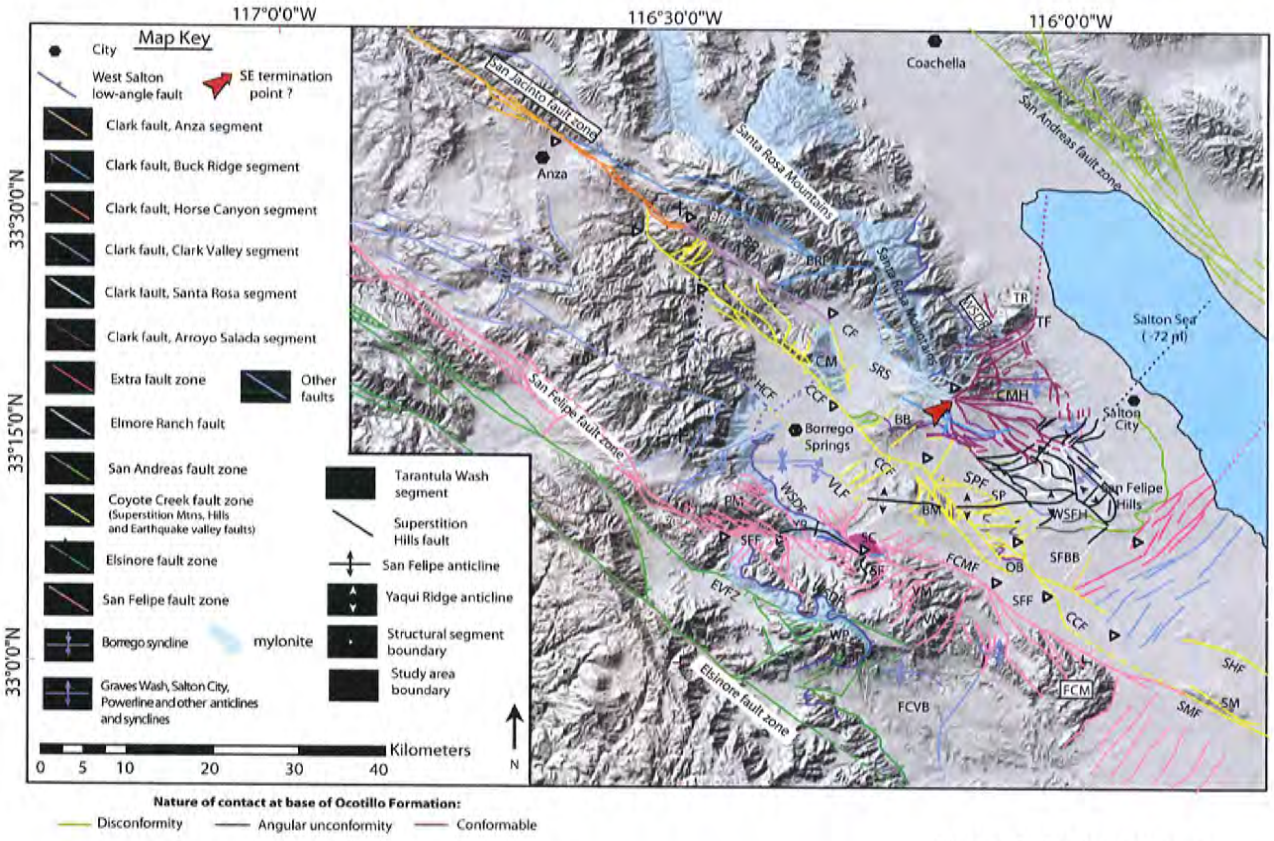

Figure 3. Full caption on following page

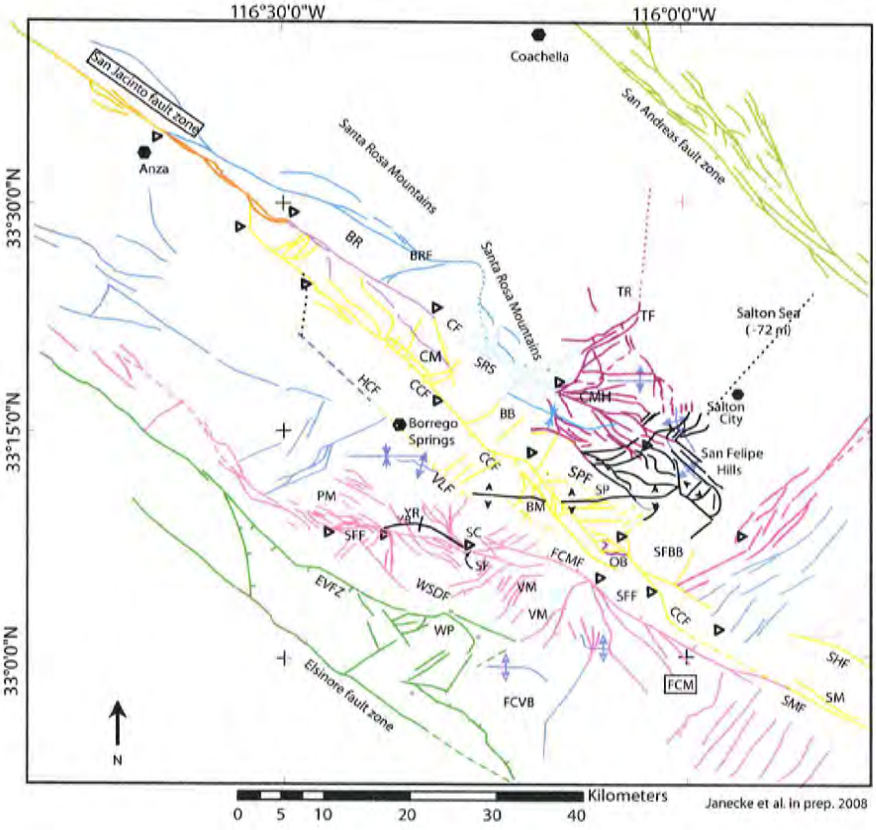

Figure 3. Map of active fault in the Borrego Springs area with structural segments added in 3b. a) Important structural features of Borrego Springs area and the nature of the basal contact of the Ocotillo Formation in the SW Salton Trough. Note that the West Salton low-angle fault is folded and cut by dextral strike-slip fault zones. 3b. Names of structural segments and positions of boundaries between them are modified from Sanders (1989), Kirby (2005), Steely (2006) and this study and are placed at major bends, steps and changes in structural style. BRF-Buck Ridge fault; NW-FCMF-NW Fish Creek Mountain fault; Segments of Clark fault: AS-Arroyo Salada segment; CVS-Clark Valley segment; HCS-Horse Canyon segment; TWS-Tarantula Wash segment; CVS-Clark Valley segment; SRS-Santa Rosa segment; Segments of Coyote Creek fault: BBS-Borrego Badlands segment; BMS-Borrego Mountain segment; CRS-Coyote Ridge segment; CS-central segment; SS-Superstitions segment; SHS-Superstition Hills segment; SMS=Superstition Mountains segment. Segments of San Felipe fault zone: GC-Grapevine Canyon segment; MBS-Mescal Bajada segment; PR-Pinyon Ridge segment NF; NW-FCMF-NW Fish Creek Mountain fault; SE-FCMF-SE Fish Creek Mountain fault. Other names: BB-Borrego Badlands; BM-Borrego Mountain; BSF-Borrego Sink fold belt; Borrego syncline-BS; BRF-Buck Ridge fault; CCF-Coyote Creek fault; CF-Clark fault; DF-Dump Fault; ER-Elmore Ranch fault; EVFZ-Earthquake Valley fault zone; FCM-Fish Creek Mountains; FCMF-Fish Creek Mountains fault; FCVB-Fish Creek-Vallecito basin; GC-Grapevine Canyon; H-Henderson Canyon fault; HC-Hell Canyon fault; KF-Kane Springs fault; OB-Ocotillo Badlands; PR-Pinyon Ridge; SFH- San Felipe Hills; SM-Split Mtn anticline; SC-Sunset conglomerate of the Ocotillo Formation; SF-Sunset fault; SFBB=San Felipe-Borrego basin; SFF-San Felipe fault; SR-Santa Rosa fault; SM-Superstition Mountain; SPF-Squaw Peak fault; SH-Superstition Hills; TB-Tierra Blanca Mountains; VLF-Veggie line fault; VM-Vallecito Mountains; VFCB= Vallecito-Fish Creek basin; WSDF-West Salton detachment fault; WP-Whale Peak; YR-Yaqui Ridge. Faults are compiled and modified from Rogers, 1965; Jennings, 1977; Kennedy and Morton, 1993; Morton, 1999; Kirby, 2005; Lutz, 2005; Kennedy, 2000; 2003; Kennedy and Morton, 2003; Morton and Kennedy, 2003; and this study. Mylonite (light blue) was modified from Sharp (1979), Kairouz (2005) and Steely (2006).

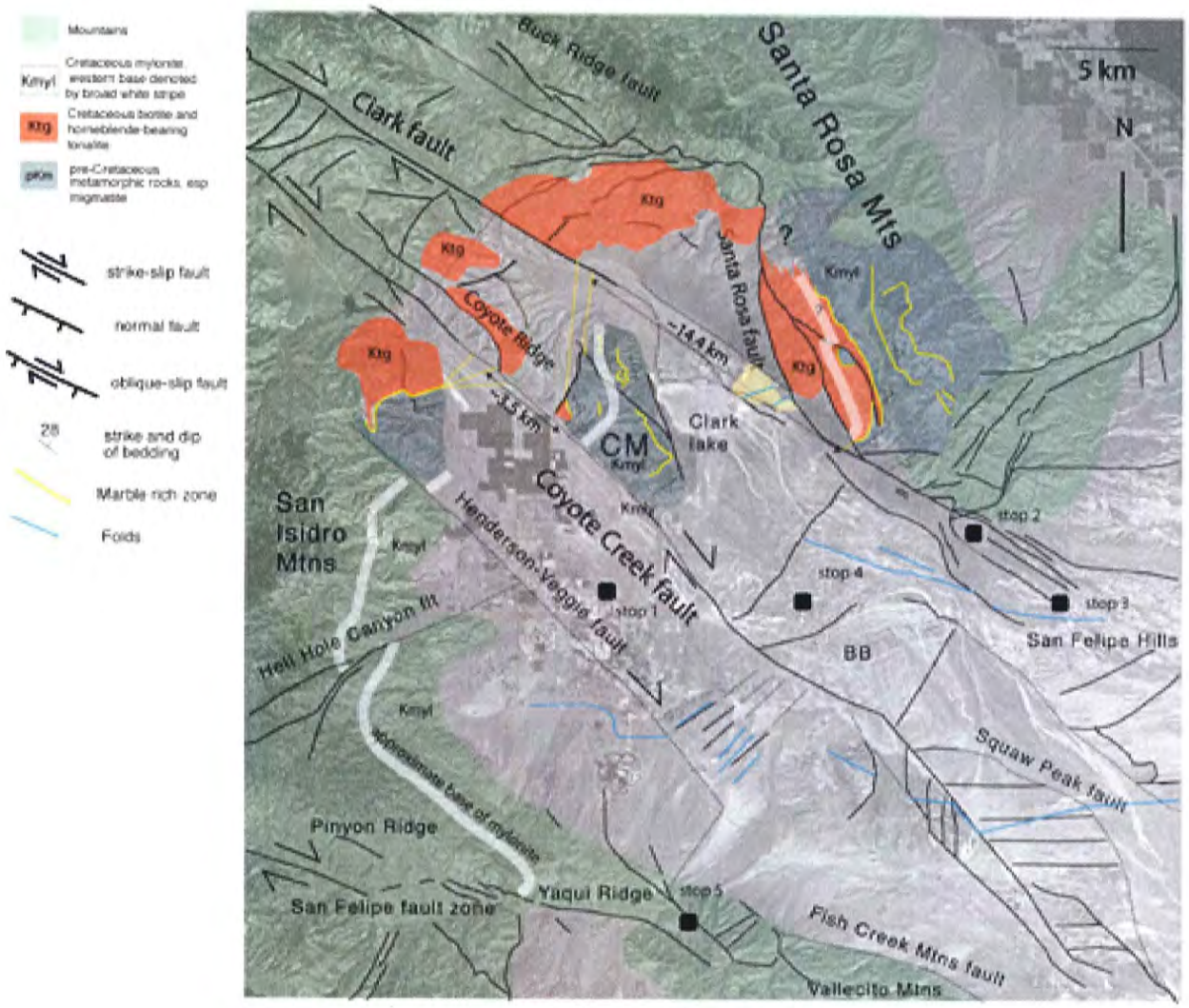

Figure 4. Simplified map showing the offset features used to determine the lifetime slip rate across the Coyote Creek and Clark faults near Coyote Mountain.

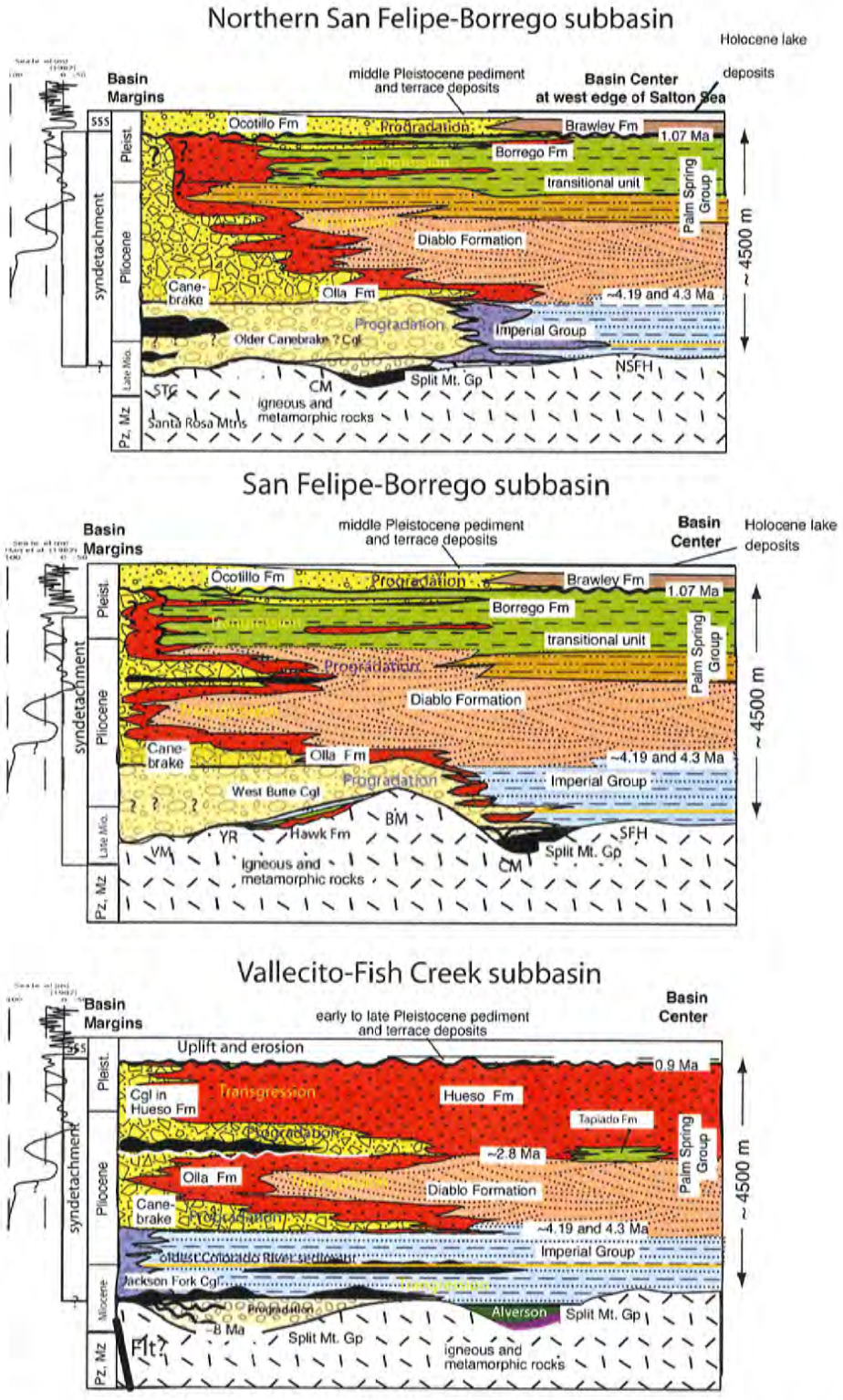

Figure 5. Simplified geologic columns of parts of the San Felipe-Borrego basin and Fish Creek-Vallecito subbasins, which show the lateral changes of formation and facies from the basin-bounding structures to the distal interior of the basin (Janecke et al., in prep.). Data from Dibblee, 1954, 1984, 1996; Winker and Kidwell, 1996; Dorsey, 2006; Dorsey et al., 2007; Kirby, 2005; Belgarde, 2007; Steely, 2006, and Janecke, unpublished mapping.

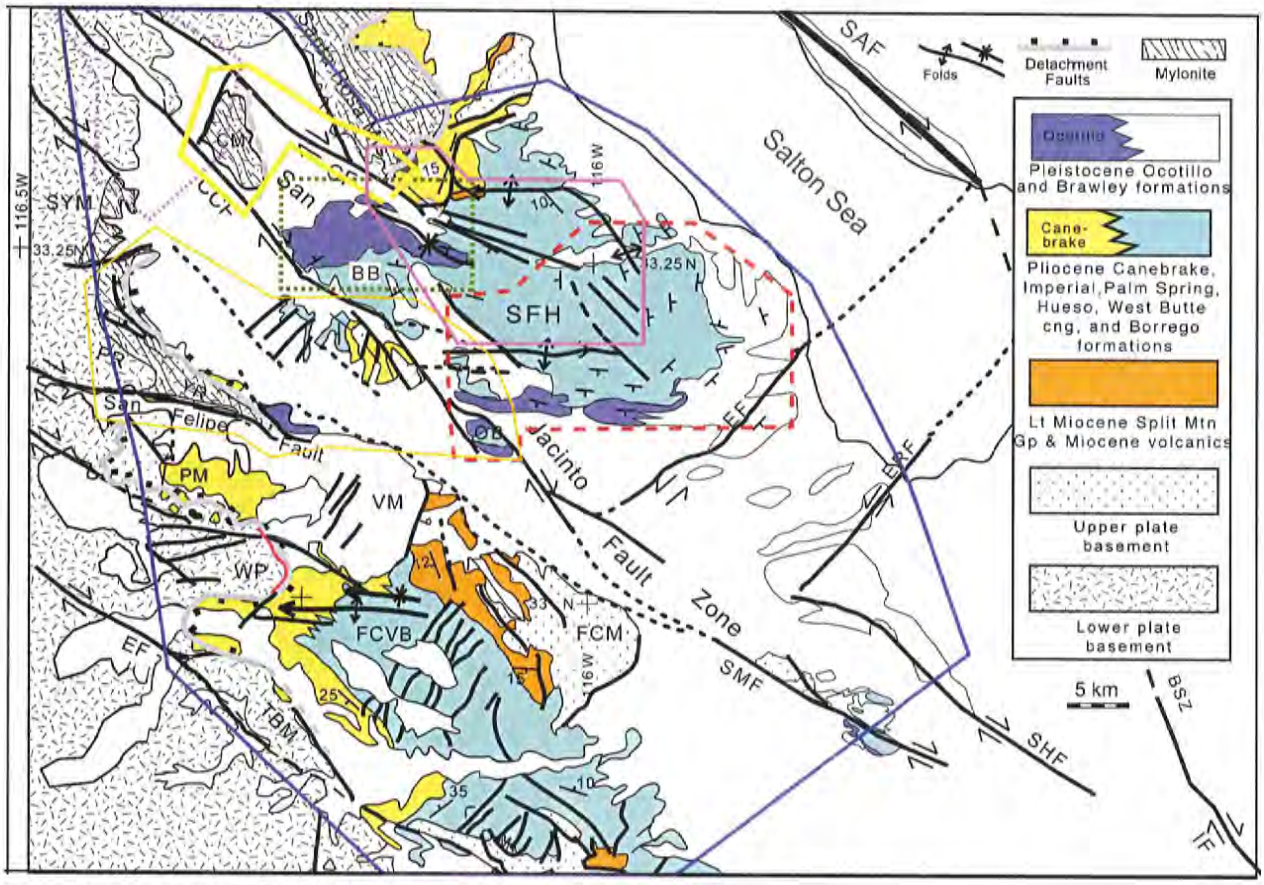

Figure 6. Regional and simplified geologic map showing the locations of recent field studies in San Jacinto and San Felipe fault zones. Kirby (2005, red outline), Lutz (2005, lime green outline), Steely (2006, orange outline), Belgarde (2007; pink outline) Forand (2010, in press), and Janecke and Dorsey (unpublished mapping 2001-2008, blue).

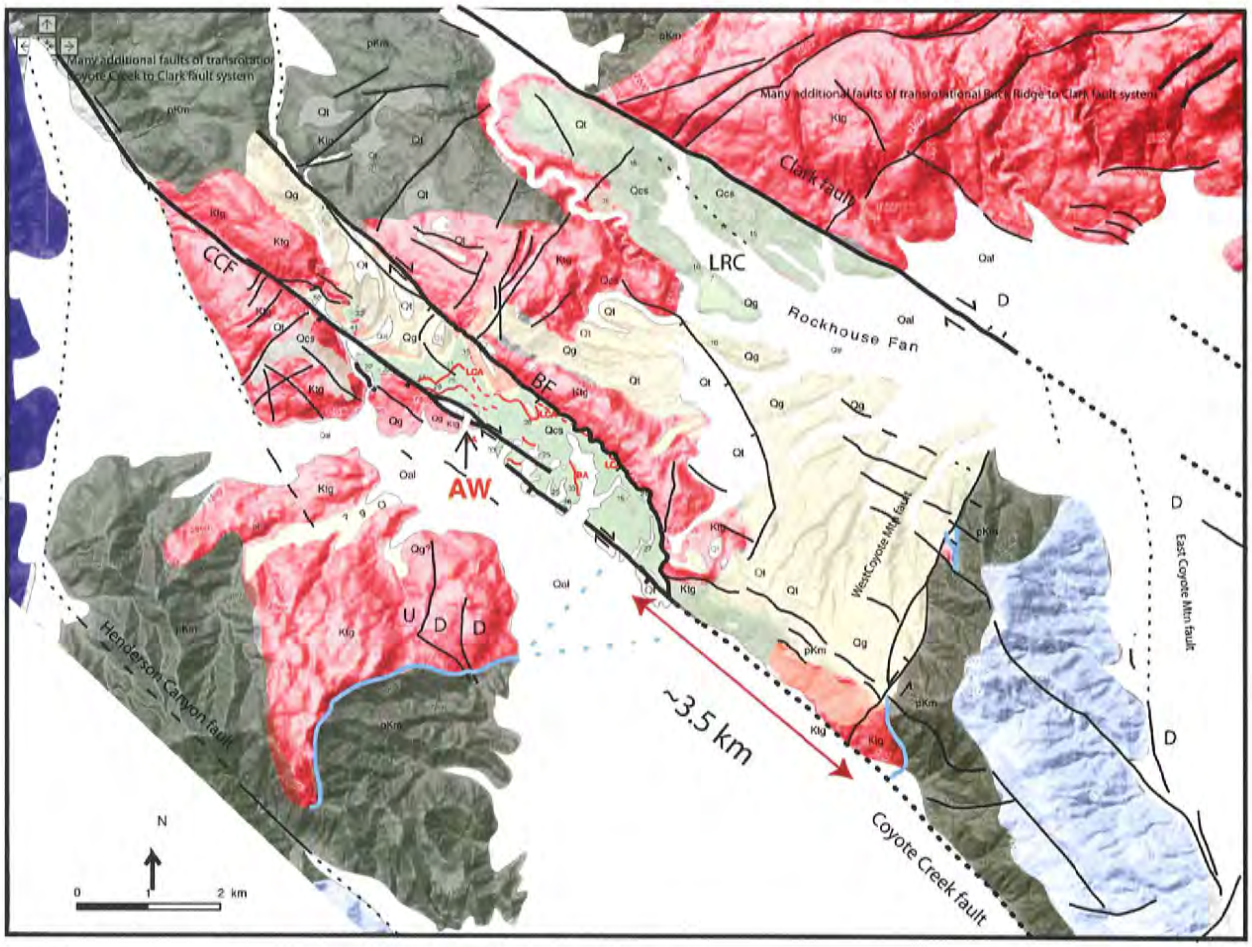

Qal Quaternary alluvium

Kmly Cretaceous mylonite

Ktg Cretaceous tonalite, granodiorite, etc.

pKm pre-Cretaceous metamorphic rocks, esp. migmatite

dissected high terrace surfaces

weakly lithified gravel

Qcs cemented conglomerate and sandstone

tonalite-clast breccia

strike-slip fault

normal fault

oblique-slip fault

28 strike and dip of bedding

marble with a Paleozoic protolith, marker horizon

AW Ash Wash
BCF Box Canyon Fault
CF Clark Fault
CCF Coyote Creek Fault
LRC Lower Rockhouse Canyon

BA, LCA Bishop and possible Lava Cree B ash

Figure 7. Geologic map of the Coyote Mountain area showing 3.5±1.3 right separation of moderately to steeply dipping metasedimentary wall rocks (olive) that wrap around a distinctive pluton (red). Mapping compiled from many sources including Dorsey, 2002 and Janecke and Forand, 2010, in press.

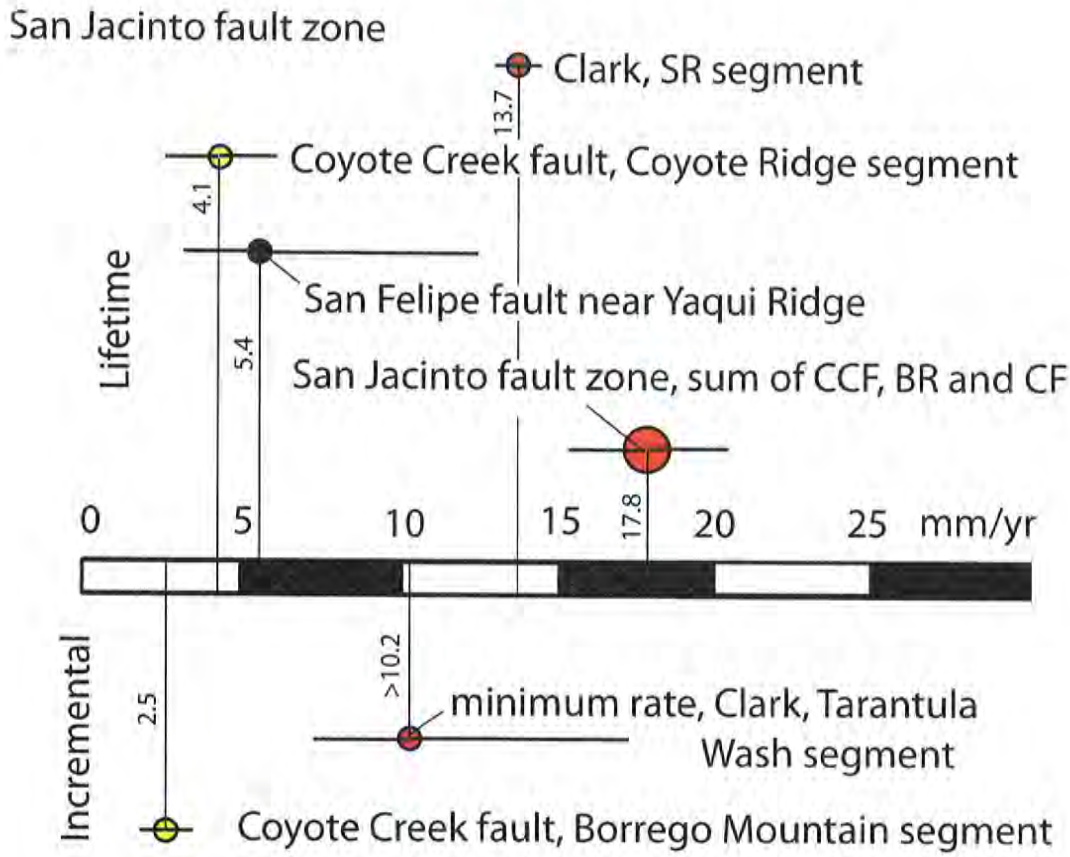

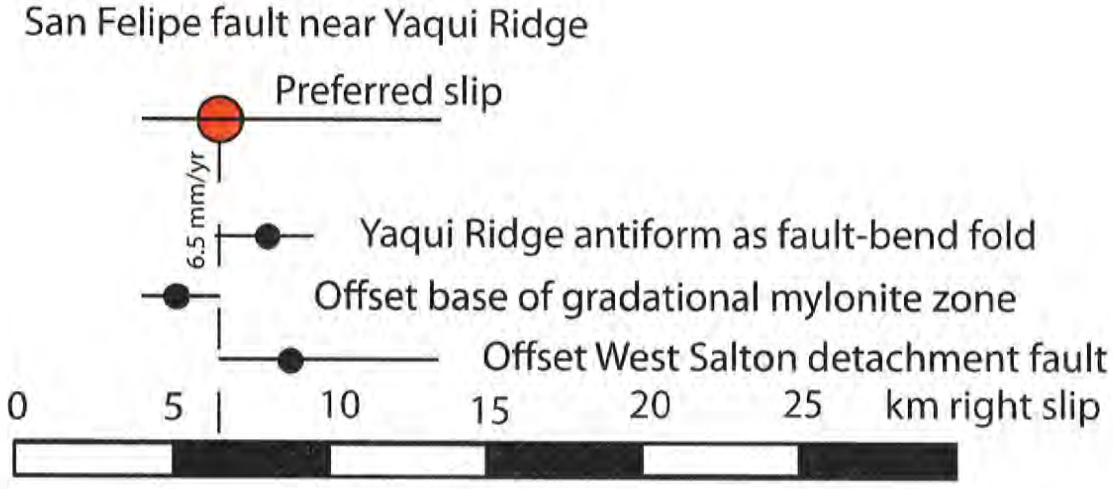

Figure 8. Graph of slip rates across the San Jacinto fault zone and San Felipe fault zone. Top: Lifetime slip rates are above the x axis and slip rates averaged over the last 0.5 m.y. are below the x axis. CCF=Coyote Creek fault, BR=Buck Ridge fault. CF=Clark fault, SR=Santa Rosa segment. Bottom: Displacement across the San Felipe fault zone near Yaqui Ridge.

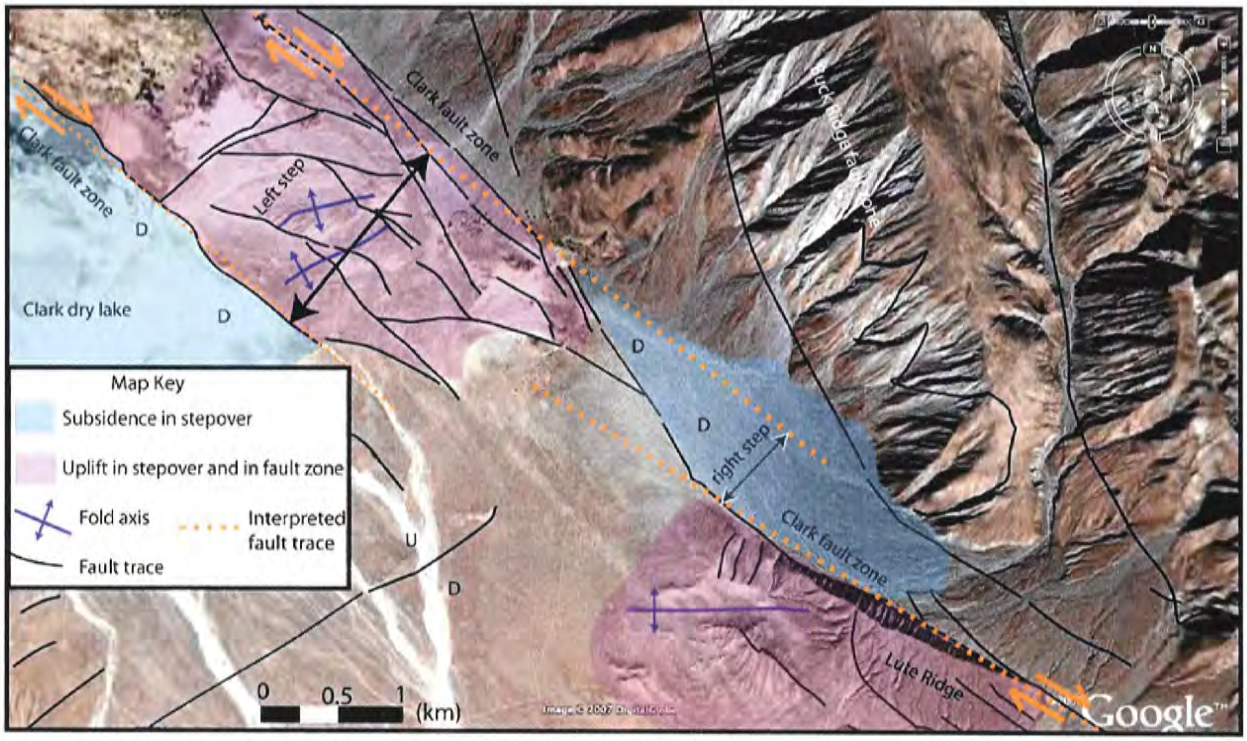

Figure 9. Google Earth image and structural relationships along the southeast part of the Santa Rosa Segment of the Clark fault of the San Jacinto fault zone. Notice the multiple steps between the fault traces, which produce both uplifting and subsiding areas along the fault zone. From Belgarde (2007) depicting the structural interpretation of Janecke.

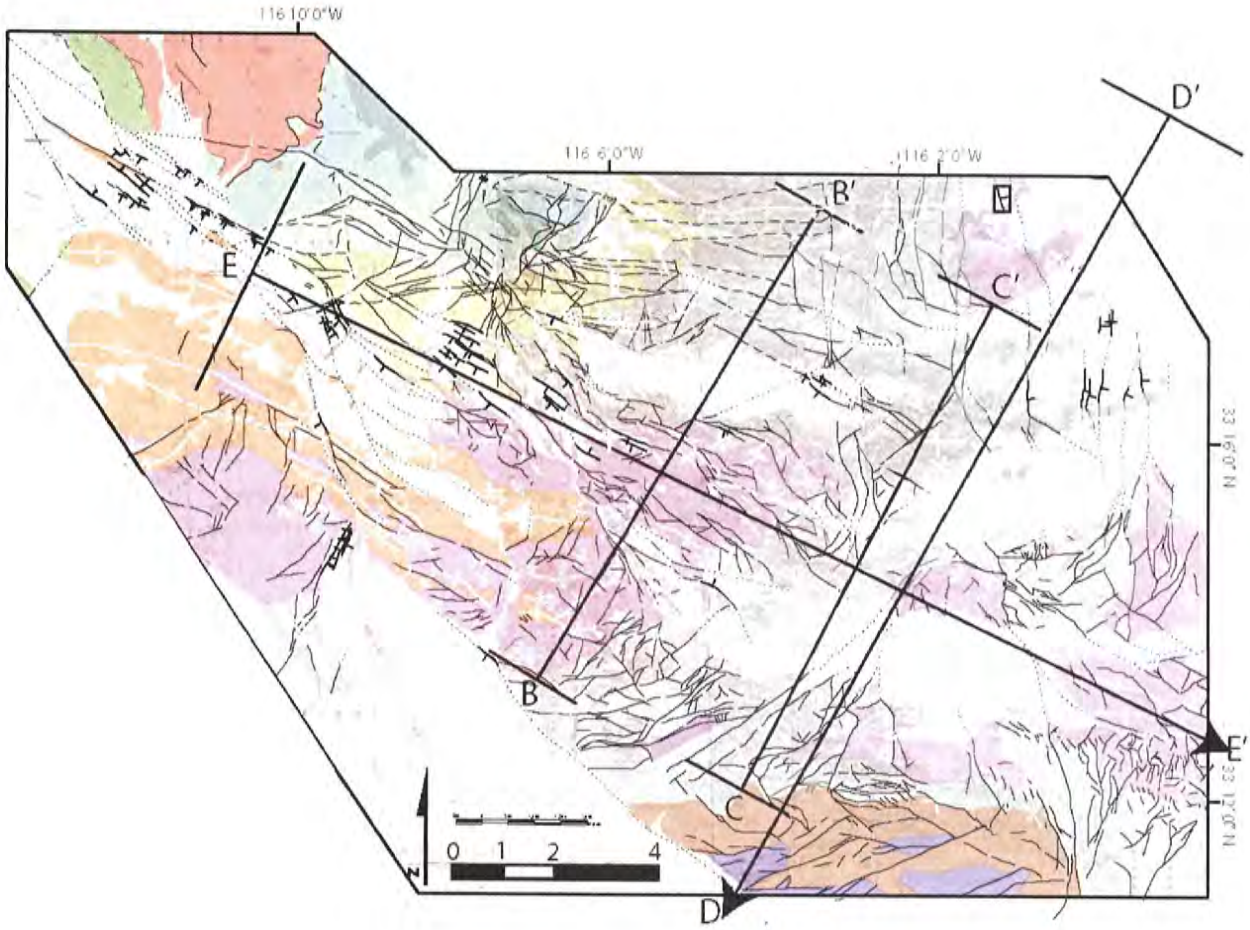

Figure 10a. Geologic map of the Santa Rosa, Arroyo Salada and part of the Tarantula Wash segments of the Clark fault (Simplified from plate 1 of Belgarde and Janecke, in Belgarde 2007). Faults are highlighted. Fault scarps are bolded

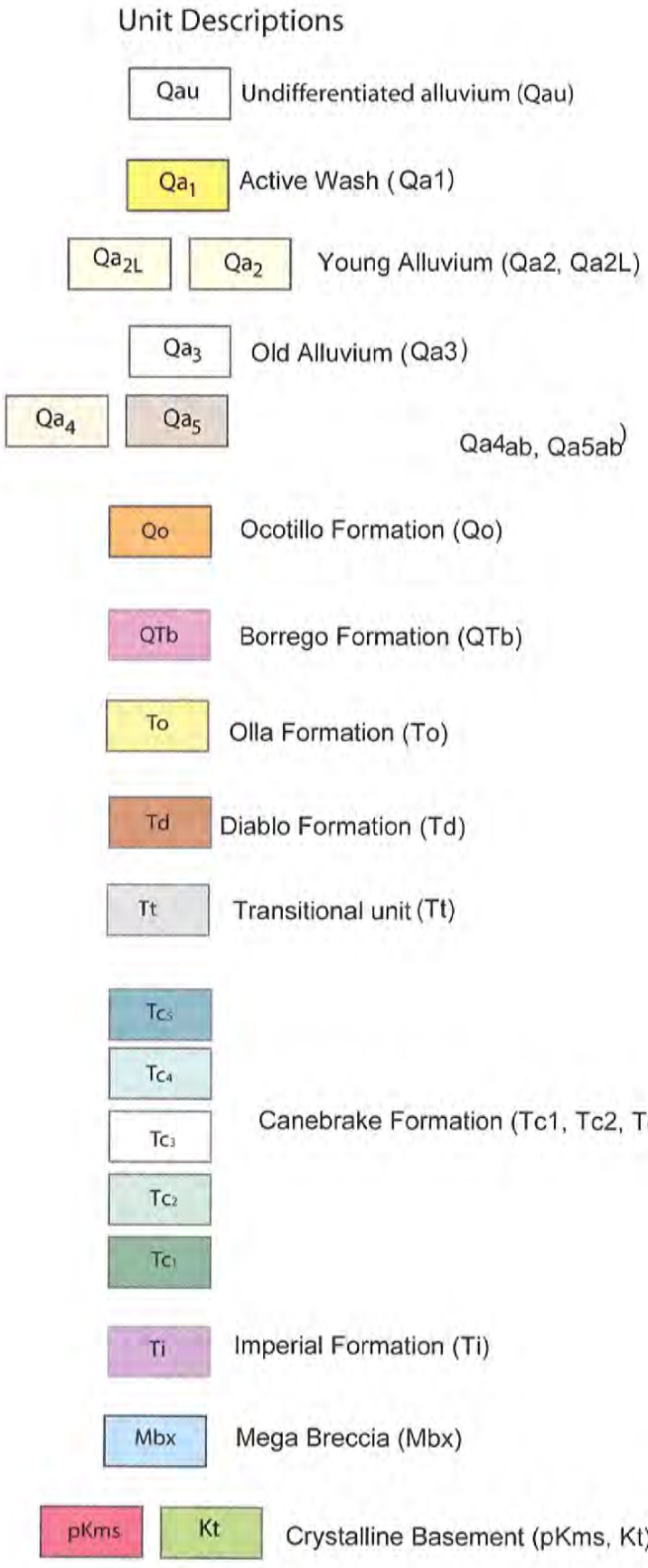

Figure 10b. Legend for figure 10a.

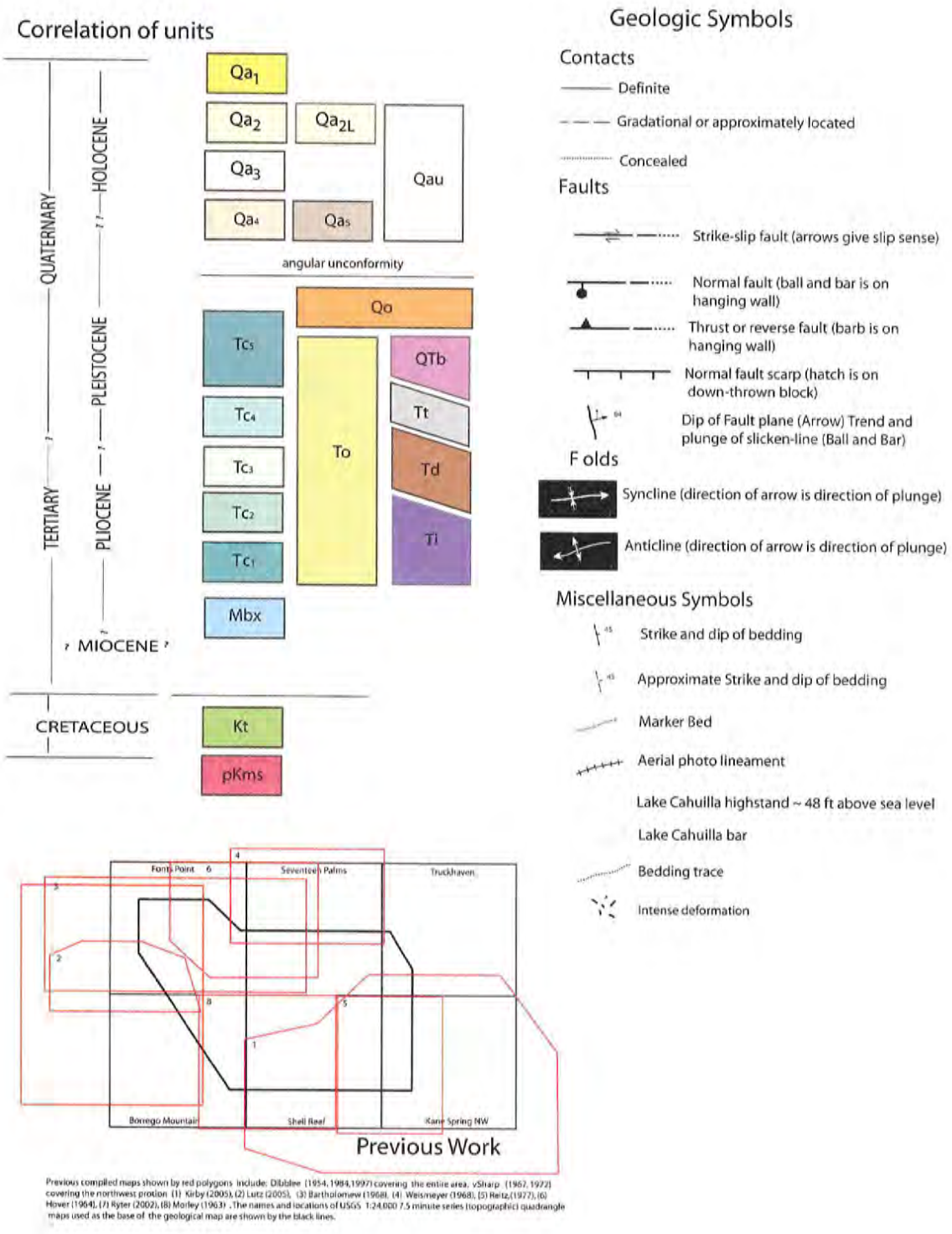

Figure 10c. Symbols, correlation of units and prior mapping.

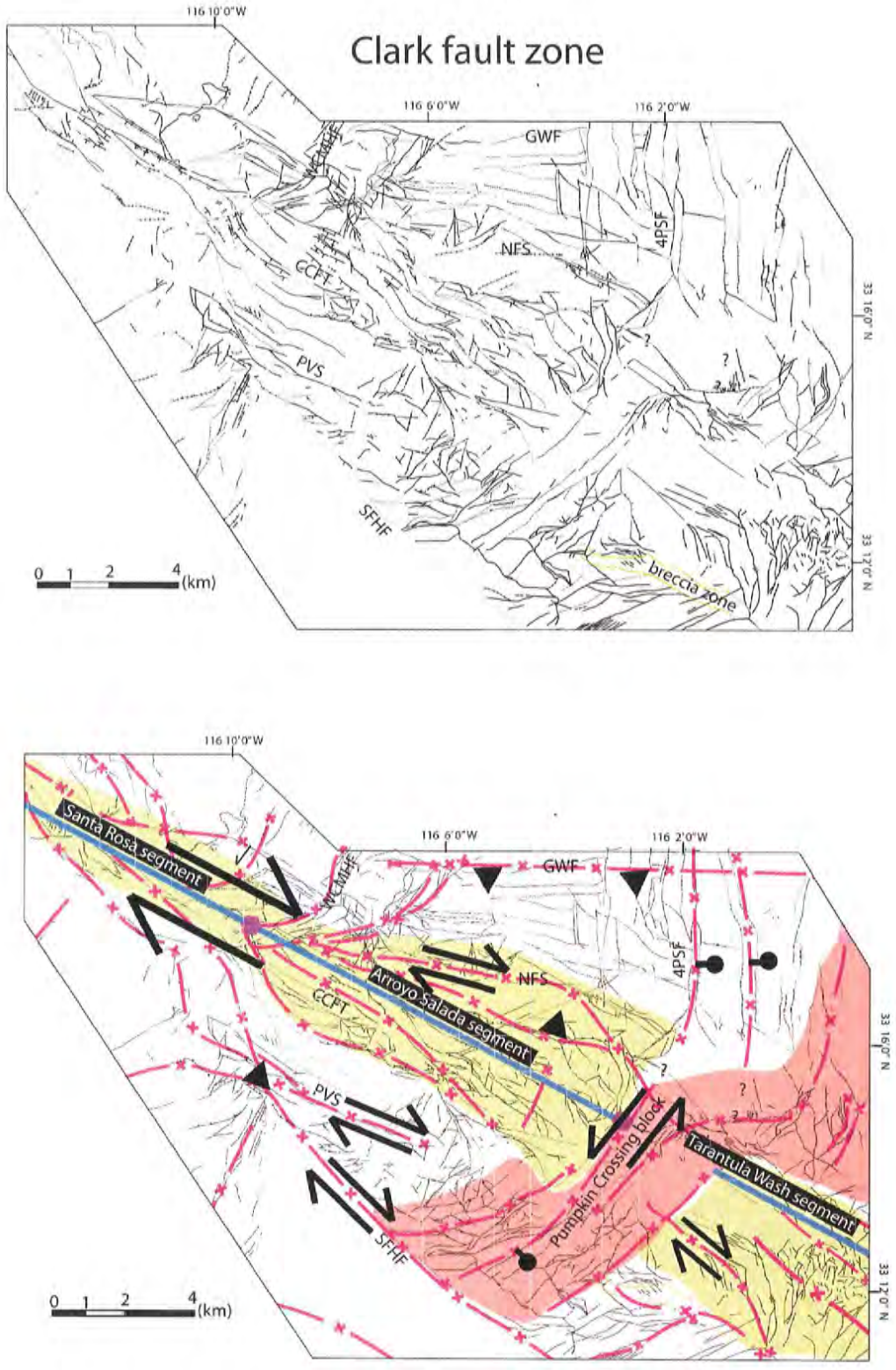

Figure 11. Simplified fault map showing the main elements of the Clark fault zone in figure 10, including the three structural segments of the fault (Belgarde and Janecke, in Belgarde 2007). Refer to figure 10 for legend and figure 3 for adjacent segments. Modified from Belgarde (2007).

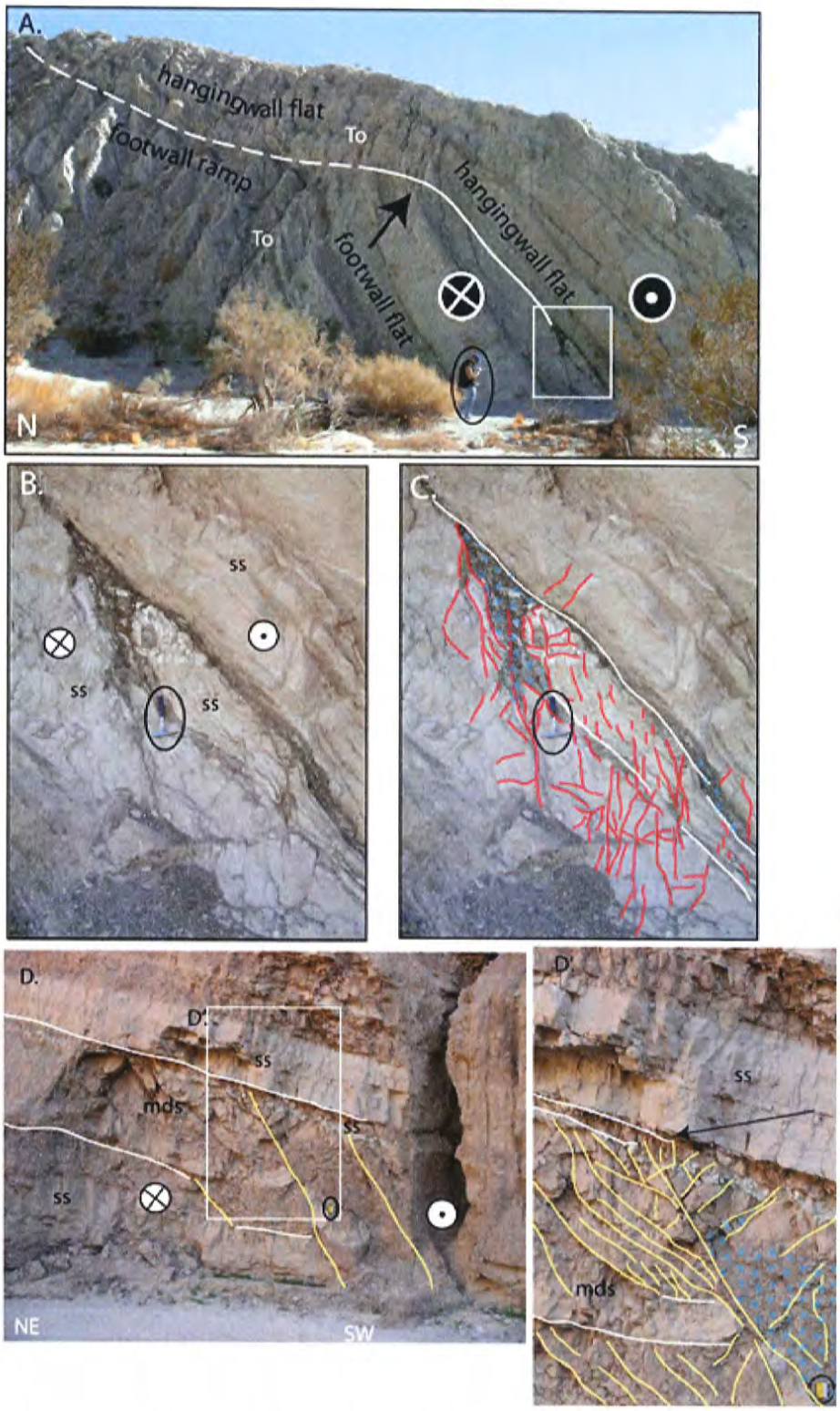

Figure 12. Stop 2. a-c Photographs looking SE along a major strand of the Clark fault with a ramp and flat geometry in Coachwhip Canyon. Clay gouge is brown and forms pods localized along a fraction of the fault zone. Elsewhere the fault is only a mm thick and is difficult to identify. From Belgarde (2007). D and D' Another example of a strike-slip fault with ramps and flats within the Arroyo Salada segment of the Clark fault.

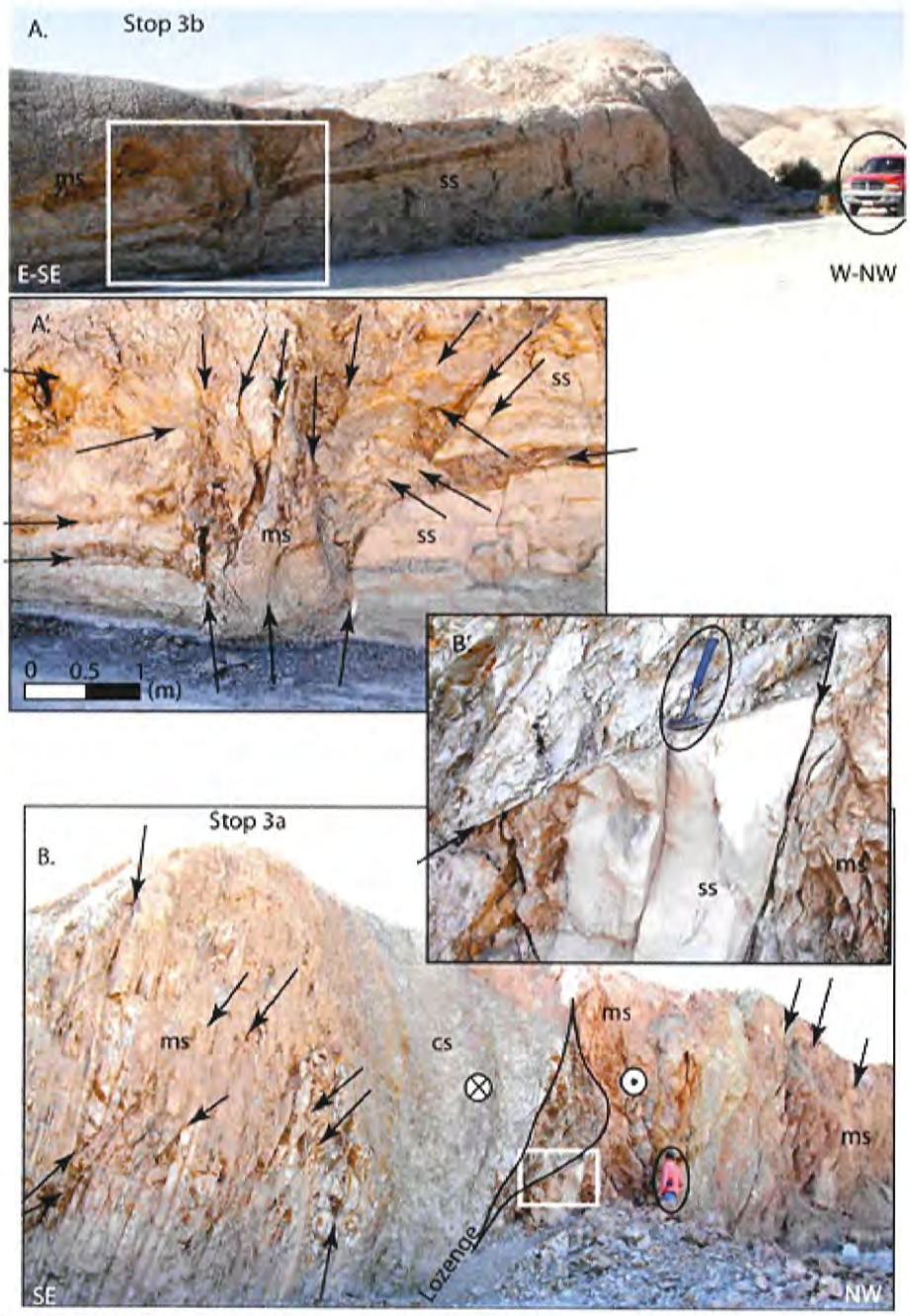

Figure 13. (A, A') Photograph looking at a left-lateral fault zone in the Clark fault zone. The fault cuts the transitional formation along the south side of Tule Wash (UTM, 0584259, 3677873). This fault has a strike of ~175° and dies out ~ 300 meters south of this outcrop. Deformation associated to the fault preferentially splays into mud-rich beds. (A) 2 m tall truck for scale (A') Close up of the fault zone, faults are indicated by the black arrows. (B, B') Photograph of an outcrop of a large fault of the Clark fault along the south edge of Arroyo Salada Wash near the 17 Palms (UTM, 0583048, 3679832). 6 ft tall person for scale. Fault zone is ~ 20 meters wide and contains multiple steep fault surfaces (black arrows) and fault blocks. The general trend of this fault trace is east-west to the east of the outcrop and the western extent is unclear due to the wash. The strike and dip of a major fault surface within this deformation zone is 65, 65° SE and the rake of slickenlines are ~ 18° E NE. (B') The 3 meter tall lozenge shaped structure in the gray claystone truncates a block of undeformed sandstone, 30 cm long hammer for scale. From Belgarde (2007).

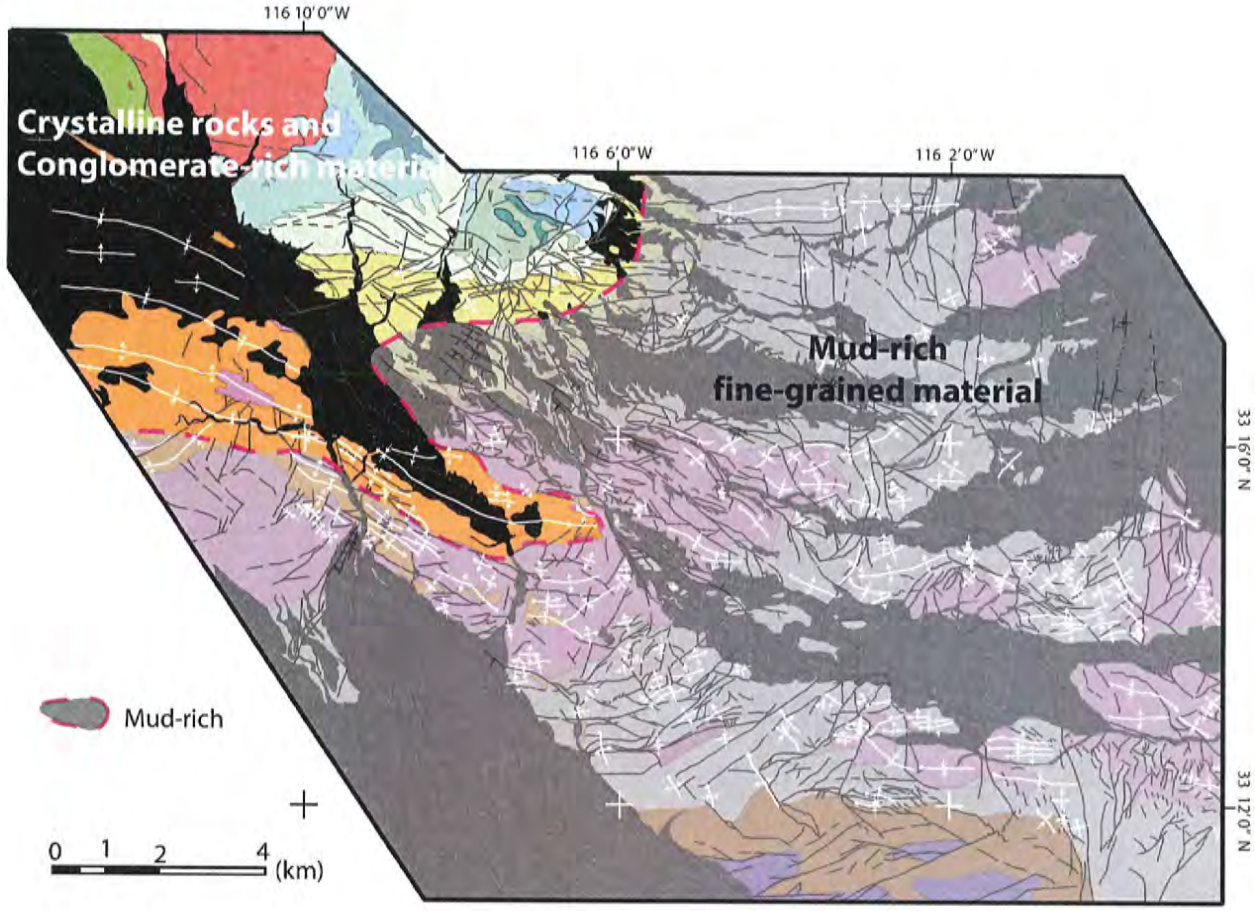

Figure 14. Geologic map highlighting the intense-folding strains in mud-rich sedimentary rocks within the Clark fault zone. Modified from Fig. 3-18 of Begarde (2007). Deposits younger than the Ocotillo Formation are black or gray. The mud-rich sedimentary rocks make up the grayed region. Notice the dramatic increase in the number and length of folds relative to the crystalline rocks (red, green) and the coarse grained sandstone to conglomerates (shades of blue and green, orange).

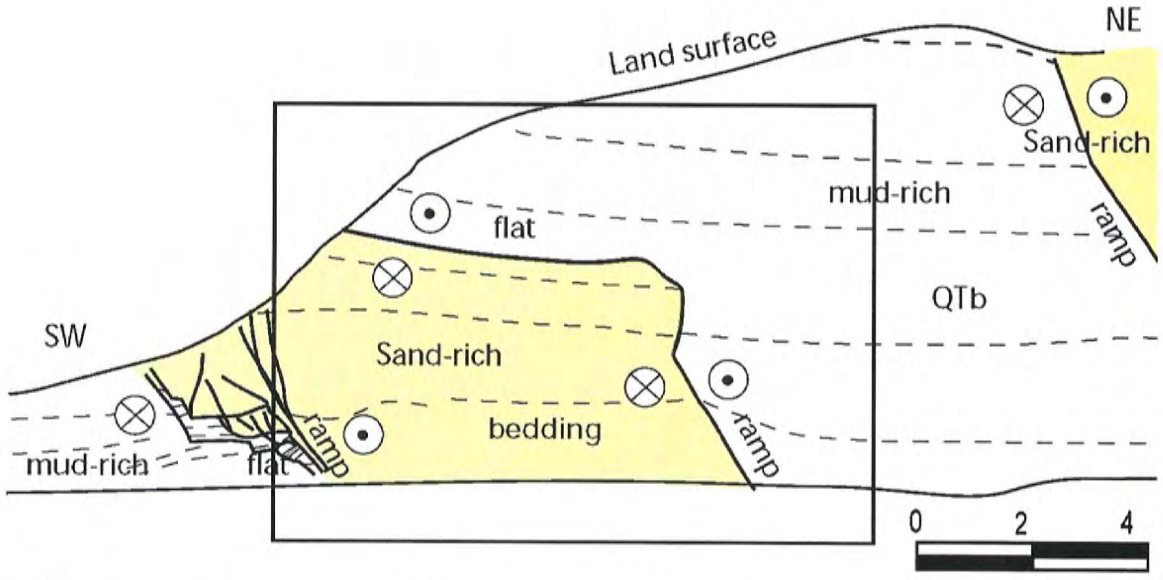

Figure 15. (a) Photograph looking NW at a major strand of the Clark fault in the Arroyo Salada segment. b) Sketch of ramp and flats in a dextral strike-slip fault zone with mud-rich (whiter) and sand-rich (yellow) sedimentary rocks. Refer to (a) for the photograph of part of this sketch. Modified from Belgarde (2007).

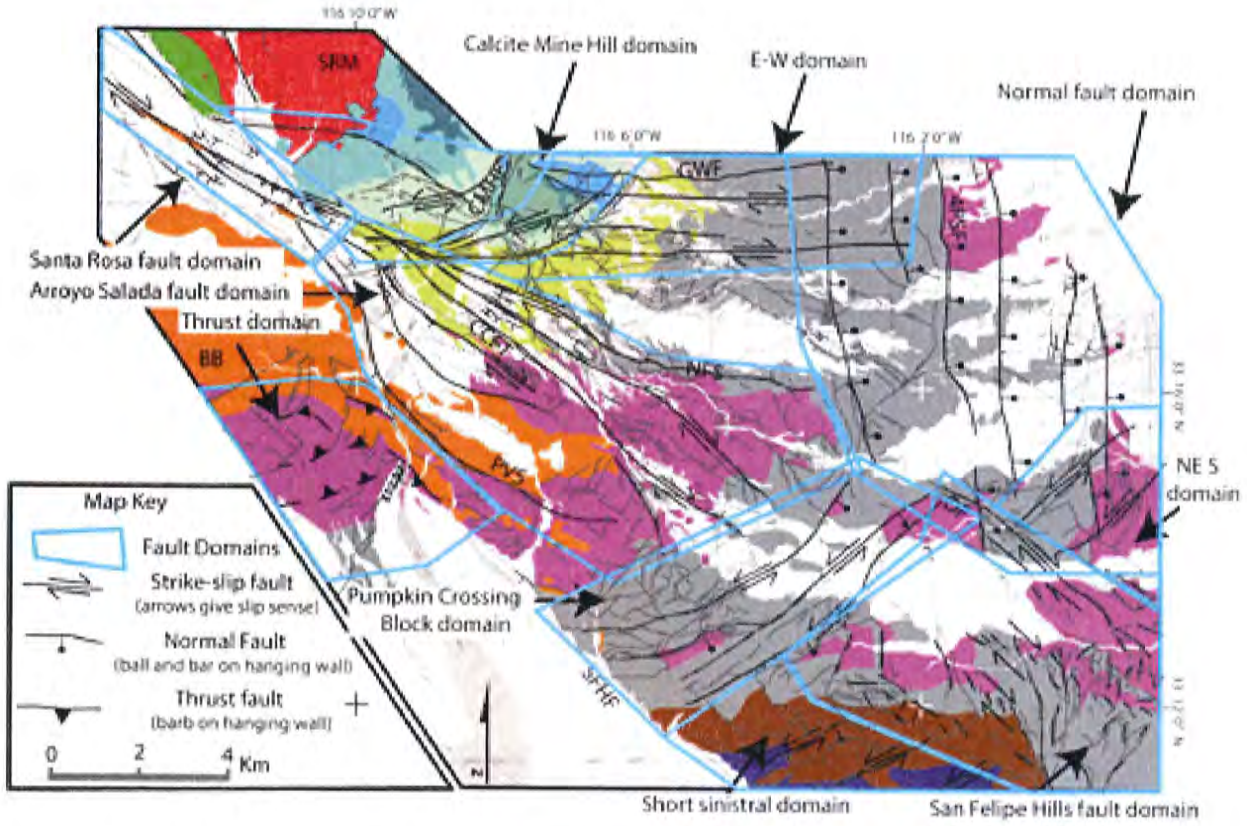

Figure 16. Map showing discrete domains with distinct fault geometries within the Clark fault zone. Refer to fig 10 for the key to the geological map in the background. Major structures that characterize each domain are indicated in black. Note that most fault domains overlap with adjacent domains because boundaries have a mappable width. SFHF-San Felipe Hills fault; NE S-is a sinistral domain; PVS- Palo Verde Splay; NFS- North Fork Splay; CCFT- Central Clark fault trace, BB- Borrego Badlands; SRM- Santa Rosa Mountains; GWF- Graves Wash fault; 4PSF- Four Palms Spring fault; DF-Dumpfault; CMHF- Calcite Mine Hill fault. Modified from Belgarde (2007).

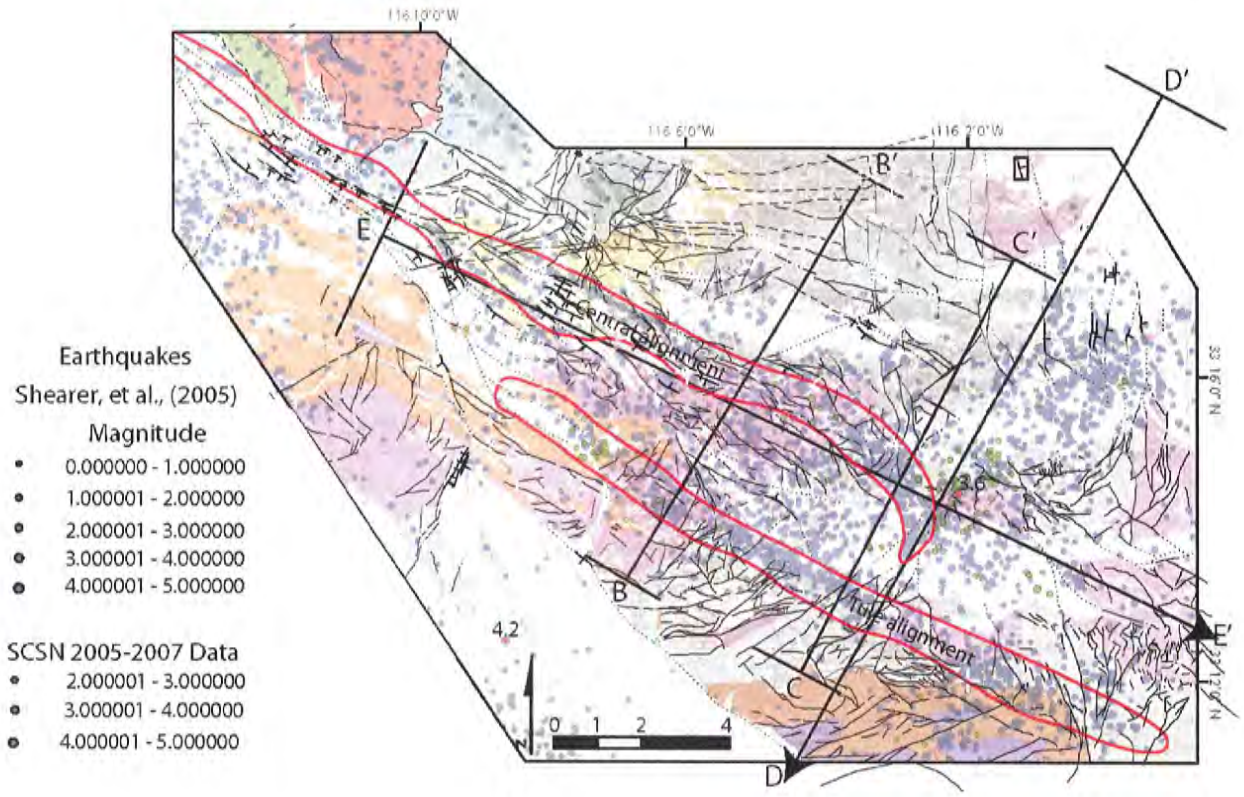

Figure 17. Correlation between microseismicity and geology of the Clark fault zone. Refer to Fig. 10 for the key to the geological map. Quaternary alluvium is white. Blue epicenters are from Shearer et al's (1982-2002) catalog and green epicenters (2002-2005) are from the SCSN catalog (Shearer et al. 2005). The most recent ML 4.2, and 3.6 earthquake epicenters are labeled and highlighted in red. Cross sections, B-B', C-C' and D-D' from figure 18 are shown. End bars on cross sections represent width of selection zone. Note the excellent correlation between faults mapped at the surface and earthquakes along the Central alignment. There is a clear mismatch between the Tule Wash alignment of earthquakes at 8-12 km depth and mapped structures above it. Modified from Belgarde (2007).

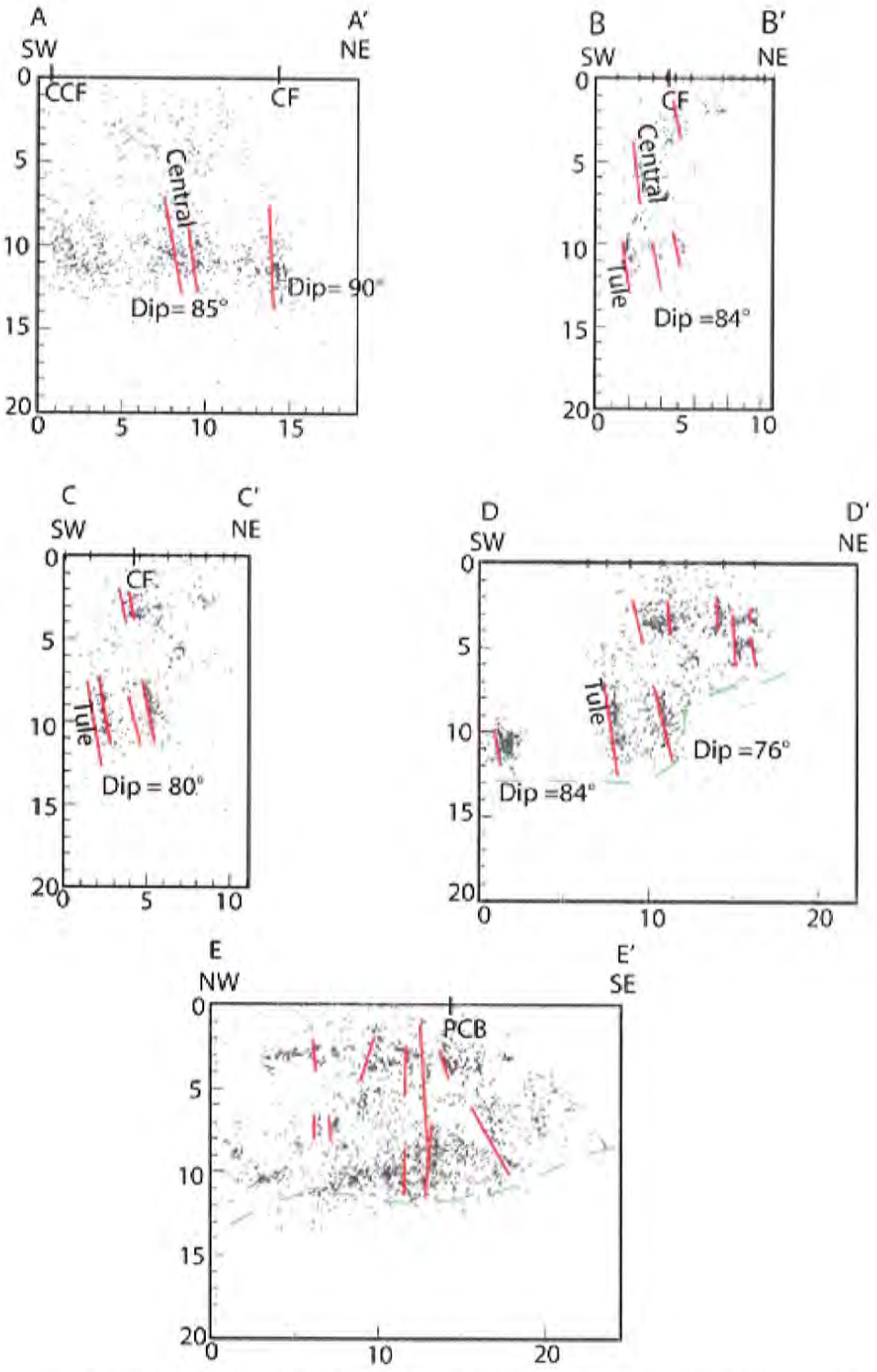

Figure 18. Cross sections of microseismicity along the Clark fault zone. Red lines are parallel to earthquake alignments, green denotes the base of seismogenic zone, black indicates where fault traces intersect each cross section, and major fault traces are labeled, CF- Clark fault; CCF- Coyote Creek fault; PCB - Pumpkin Crossing block. Widths of the selection zones for each cross section are, A-A': 5 km, B-B': 2 km, C-C': 2 km, D-D': 3.5 km, E-E' 5.5 km. Modified from Belgarde (2007). Data from Shearer et al. (2005).

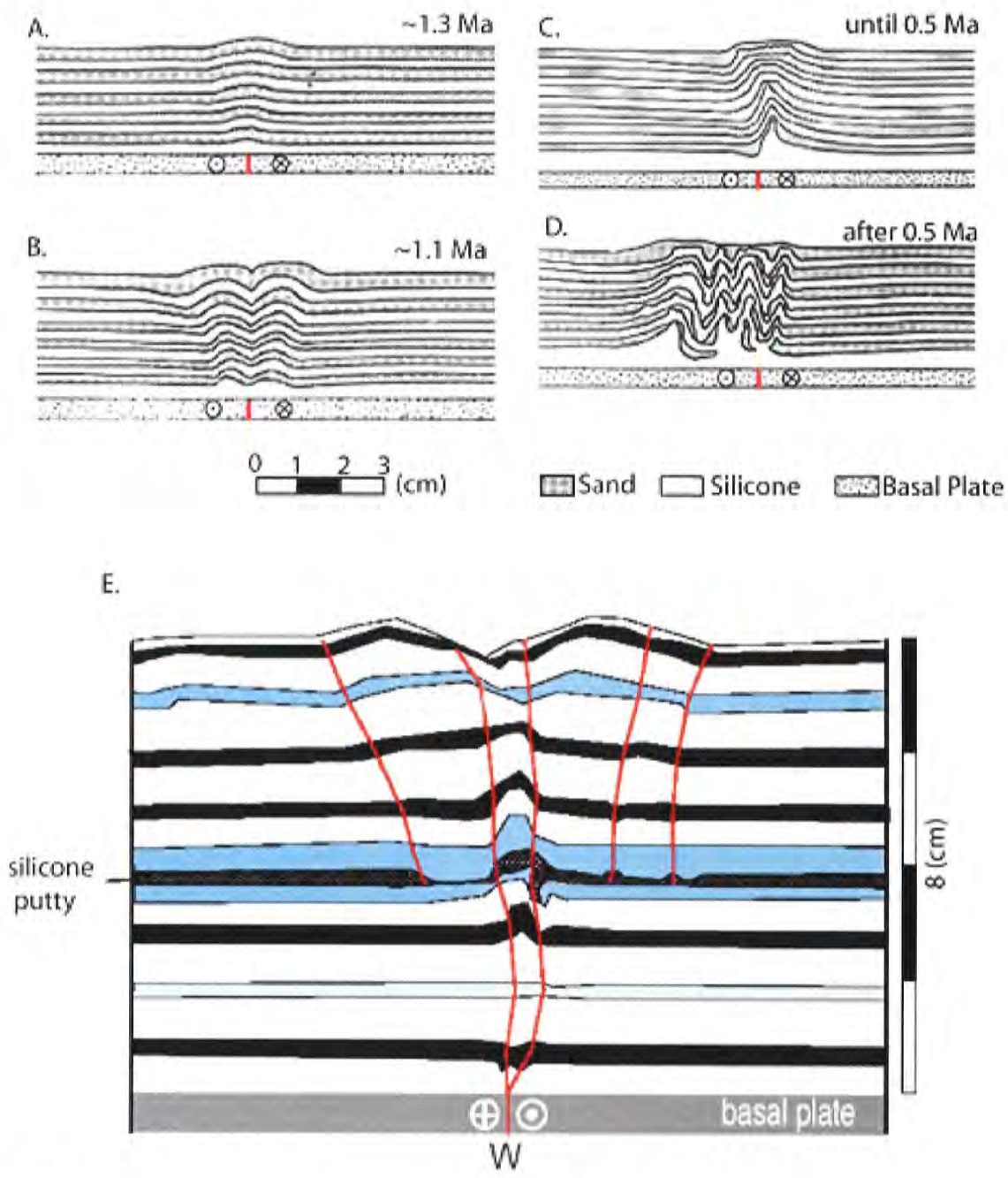

Figure 19. Cross sectional views of laboratory experiments of strike-slip faults that deform sedimentary rocks above a rigid substrate. A-D from Richard et al. (1995). Cross section of models. The section lines are perpendicular to the strike-slip fault. The Clark fault is inferred to have have the geometry in figures a-d at the times indicated (Kirby et al., 2007). Experiments (A), (B), and (C) are shown after 8 cm of left lateral displacement; experiment (D) after 20 cm of left-lateral offset. (E) Model from Le Guerroué and Cobbold unpublished data included with permission. Cross section of a block model containing a detachment horizon made of silicone putty. Folding and related faulting due to strike slip motion of the basal plate is depicted in this cartoon of the original sandbox model. A "pitch-fork" shaped fault zone formed as a result of inserting a weak silicone layer. From Belgarde (2007).

Figure 20. Stop one. The view northward at Anza's Angel. The white streak is a marble between gray tonalite below and rusty biotite-rich migmatite above. Orange groves are in the foreground.

Figure 21. Stop one. Photograph looking northeast at the same marble-rich interval as depicted in figure 20. Here it is high up in the southeast Santa Rosa Mountains. This white marble-rich zone also marks the contact between gray tonalite below and rusty biotite-rich migmatite above.